arXiv:2003.12233v1 [q-bio.CB] 27 Mar 2020

PDE MODELS OF ADDER MECHANISMS IN CELLULAR PROLIFERATION

MINGTAO XIA*, CHRIS D. GREENMAN†, AND TOM CHOU‡

Abstract. Cell division is a process that involves many biochemical steps and complex biophysical mechanisms. To simplify the understanding of what triggers cell division, three basic models that subsume more microscopic cellular processes associated with cell division have been proposed. Cells can divide based on the time elapsed since their birth, their size, and/or the volume added since their birth – the timer, sizer, and adder models, respectively. Here, we propose unified adder-sizer models and investigate some of the properties of different adder processes arising in cellular proliferation. Although the adder-sizer model provides a direct way to model cell population structure, we illustrate how it is mathematically related to the well-known model in which cell division depends on age and size. Existence and uniqueness of weak solutions to our 2+1-dimensional PDE model are proved, leading to the convergence of the discretized numerical solutions and allowing us to numerically compute the dynamics of cell population densities. We then generalize our PDE model to incorporate recent experimental findings of a system exhibiting mother-daughter correlations in cellular growth rates. Numerical experiments illustrating possible average cell volume blowup and the dynamical behavior of cell populations with mother-daughter correlated growth rates are carried out. Finally, motivated by new experimental findings, we extend our adder model cases where the controlling variable is the added size between DNA replication initiation points in the cell cycle.

Key words. PDE, structured populations, cell size control

AMS subject classifications. 35Q80, 92B05, 92C37

1. Introduction.

How cells regulate and maintain their sizes, as well as sizes of their appendages is a longstanding research topic in cell biology. Besides growth of an individual cell, the size distributions within a population of cells are also a quantity of interest. When considering proliferating cell populations, individual cell growth is interrupted by cell division events that generate smaller daughter cells. The biological mechanisms that control when and how a cell divides are complex and involve many steps such as metabolism, gene expression, protein production, DNA replication, chromosomal separation (for eukaryotic cells), and fission or cell wall formation [27, 13, 4, 3, 6]. These processes are regulated and may involve intricate biochemical signaling.

Despite the complexity of cell growth and the cell cycle, three simple hypotheses for the underlying mechanisms of cell division have been proposed. Cell division can be governed by cell age a, cell volume x [26], or added volume since birth y [29, 28]. The division mechanism employed by a type of cell may be interrogated by tracking the volumes x, added volumes y, and ages a during division events. Volume growth of an individual cell can be straightforwardly measured and can be modeled by an effective empirical law such as $\dot{x} = g(a, x, y, t)$. A commonly used approximation that is supported by observations is the exponential growth law $g(x) = \lambda x$ [24].

To describe population-level distributions, PDE approaches have been developed. For example, the timer model, in which the cell division rate depends only on age of the cell is described by the classic McKendrick equation for $n(a, t)$, the expected density of cells at age a and time t [19, 9]. The McKendrick "transport" equation for the cell density takes the form $\partial_t n(a,t) + \partial_a n(a,t) = -(\mu(a) + \beta(a))n(a,t)$, in which $\beta(a)$ and $\mu(a)$ are age-dependent birth and death rates, respectively. The associated boundary condition $n(t,0) = 2\int_0^a \beta(s)n(s,t)\mathrm{d}s$ describes the birth of zero-age cells. Fully demographically stochastic versions of the timer model have also been recently developed [12, 5, 11].

The timer (or age-dependent) model does not explicitly track cell sizes, but PDE models incorporating sizer mechanisms have been developed [22, 8, 23]. In these studies size-dependent birth rates $\beta(x)$ are pertinent. Depending on the form of $\beta(x)$, cells can diverge in size x in the absence of death [16]. Existence and uniqueness of weak solutions to timer and sizer models have been proved for certain boundary and initial conditions. These types of structured population equations can be partially solved using the method of characteristics but the boundary conditions can only be reduced to a Volterra-type integral equation [22, 5].

Much like a general growth law $g(a, x, y, t)$ that can depend on age, size, added size, and time, the three distinct mechanisms of cell division need not be mutually exclusive. In this paper, we mainly focus, at the cell population level, on the cell division mechanism that incorporates the added volume, or the so-called the "adder." This mechanism, in which the cell seems to use added size as the factor controlling its division, has been indicated in many recent experimental studies. Specifically, apart from the sizer and the timer models, the adder mechanism has been recently shown to be consistent with E. coli division [27, 28, 29] and can be motivated by an initiator accumulation mechanism distinct from those used to justify sizers or timers [28, 4].

*Department of Mathematics, UCLA, Los Angeles, CA, USA
†School of Computing Sciences, University of East Anglia, Norwich, UK
‡Depts. of Computational Medicine and Mathematics, UCLA, Los Angeles, CA, USA

We will introduce the PDE model that describes cell population structure under the adder mechanism, which we describe as the "adder-sizer" PDE model, and show its connection to the classical "timer-sizer" PDE model that involves cell age and size as controlling parameters. The proof of the existence and uniqueness of a weak solution to the proposed three-dimensional "adder-sizer" PDE turns out to be more complex than the proof for the timer and/or sizer counterparts [22]. Our proof leads to the convergence of the numerical solutions to the adder-sizer PDE, allowing us to numerically evaluate the corresponding structured cell populations, facilitating further analysis, exploration of possible "blowup" behavior, and generalizations of the model. Stochastic Monte-Carlo simulations of the corresponding stochastic process are also generated and compared with numerical results for $n(x, y, t)$ and division-event densities.

Next, we propose an extension to the adder-sizer model that incorporates cellular growth rates that are correlated across successive generations. Changes in growth rates at the single-cell level have been explored using stochastic mapping methods [7, 18]. By numerically solving the PDE, we found out that the population-averaged growth rate are larger when correlations between mother and daughter cell growth rates are larger. Finally, we generalized the adder model to include a different two-phase PDE system which could describe the latest "initiation adder" mechanism, which states that the added mechanism takes effect on the cell's size at initiation instead of division in [25]. In contrast to the single-PDE division adder model, a model describing the initiation adder mechanism requires two coupled PDEs.

To model cell size control, stochastic maps that relate daughter cell sizes to mother cell sizes have been developed [17, 21]. These models describe how cell sizes evolve with generation and can interpolate among timer, sizer, and adder mechanisms. Kessler and Burov [17] assumed stochastic growth which lead to a stochastic map with multiplicative noise. They found that an adder mechanism can admit "blow-up" in which the expected cell sizes can increase without bound with increasing generation observed experimentally in filamentous bacter. Modi *et al.* [21] assume additive noise and do not find blow-up in an adder model. Stochastic maps of generational cell size do not describe population-level distributions in size or age.

2. Adder-sizer PDE models. Here, we introduce adder-sizer PDE models and generalize them to describe recently observed characteristics of population-level bacterial cell division. An adder-sizer model is one that incorporates a cell division rate $\beta(x, y, t)$ and a single-cell growth rate $g(x, y, t)$ that, instead of depending on a cell's age a, are functions of cell size x and a cell's volume *added since birth* y. Such an adder-sizer PDE model can be developed by defining $n(x, y, t)\mathrm{d}x\mathrm{d}y$ as the mean number of cells with size in $[x, x + \mathrm{d}x]$ and added volume in $[y, y + \mathrm{d}y]$. As cells have finite size and their added volume must be less than total size, $n(x \leq 0, y, t) = n(x, y \geq x, t) = 0$. A derivation similar to that given in [20] for the sizer model yields a transport equation of the form

$$\frac{\partial n(x,y,t)}{\partial t} + \frac{\partial [g(x,y,t)n(x,y,t)]}{\partial x} + \frac{\partial [g(x,y,t)n(x,y,t)]}{\partial y} = -\beta(x,y,t)n(x,y,t) \tag{2.1}$$

for the adder-sizer PDE. Here, we have neglected the effects of death, which can be simply added to the right-hand-side of Eq. 2.1.

To explicitly outline our general derivation, consider the total population flux into and out of the size and added size domain Ω shown in Fig. 1(a) and define $\tilde{\beta}(x', y', z', t)\mathrm{d}z'$ as the rate of fission of cells of size x' and added size y' to divide into two cells, one with size in $[z', z' + \mathrm{d}z']$ and the other with size within $[x' - z', x' - (z' + \mathrm{d}z')]$. For binary fission, conservation of daughter cell volumes requires $\tilde{\beta}(x', y', z', t) \equiv \tilde{\beta}(x', y', x' - z', t)$. This differential division function allows mother cells to divide into two daughter cells of differing sizes (asymmetric division), a process that has been observed in numerous contexts [14, 13, 2]. We also assume that daughter cells must have positive size so $\tilde{\beta}(x', y', z' = 0, t) = \tilde{\beta}(x', y', z' = x', t) = 0$.

The change in the number of cells in Ω due to fission can arise in a number of ways. First, if a cell in Ω divides, it can only produce two cells with size less than x. Thus, such fission events lead to a net change of $+1$ in the number of cells with $y = 0$ and size in $[0, x]$. If a cell with size within $[0, x]$ but with added size $> y$ divides, it creates two cells with added size $y = 0$ and size within $[0, x]$, leading to a net change of $+2$ cells.

For cells with any added size $y' > 0$ but with size $x' > x$, we have two subcases. If the dividing cell has size $x < x' < 2x$, it will produce one daughter cell in Ω if a daughter cell has size $0 < z' < x' - x$ or $x < z' < x'$ as shown in Fig. 1(b). If $x' - x < z' < x$, both daughter cells have size $< x$. Finally, if the dividing cell has size $x' > 2x$, at most one daughter will have size $x' < x$ (see Fig. 1(b)). Upon simplifying the above birth terms by using $\int_0^{x'} \mathrm{d}z' = \int_0^x \mathrm{d}z' + \int_x^{x'} \mathrm{d}z'$ for $x' > x$ and the symmetry $\tilde{\beta}(x', y', z', t) = \tilde{\beta}(x', y', x' - z', t)$, we combine terms to balance proliferation with transport and find

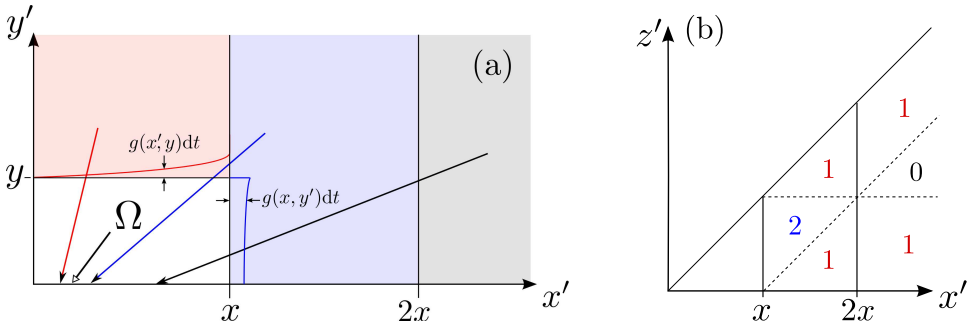


Fig. 1: The size and added-size state space for cell populations. The expected total number of cells at time t with added size within $[0, y]$ and volume (or "size") within $[0, x]$ is defined as $N(x, y, t)$. Over an increment in time $\mathrm{d}t$, the domain $\Omega = [0, y] \times [0, x]$ infinitesimally distorts $\Omega \to \Omega + \mathrm{d}\Omega$ through the growth increment $g\mathrm{d}t$. The total population within this distorted domain changes only due to birth and death. Cells within Ω that divide always give rise to two daughters within Ω, leading to a net change of $+1$ cell. (b) The z' and x' domains of the differential birth rate function $\tilde{\beta}(x', y', z', t)$. Cells outside of Ω can contribute a net $+1$ or $+2$ cells in Ω depending on the division patterns defined in the depicted regions.

$$\begin{aligned}\int_0^x \mathrm{d}x' \int_0^y \mathrm{d}y' \, \frac{\partial n(x', y', t)}{\partial t} + \int_0^x \mathrm{d}x' \, g(x', y, t) n(x', y, t) + \int_0^y \mathrm{d}y' \, g(x, y', t) n(x, y', t) \\ = \int_0^\infty \mathrm{d}y' \int_0^x \mathrm{d}x' \int_0^{x'} \mathrm{d}z' \, \tilde{\beta}(x', y' z', t) n(x', y' t) \\ + \int_y^\infty \mathrm{d}y' \int_0^x \mathrm{d}x' \int_0^{x'} \mathrm{d}z' \, \tilde{\beta}(x', y, z', t) n(x', y', t) \\ + 2 \int_0^\infty \mathrm{d}y' \int_x^\infty \mathrm{d}x' \int_0^x \mathrm{d}z' \, \tilde{\beta}(x', y', z', t) n(x', y', t).\end{aligned} \tag{2.2}$$

Upon taking the derivatives $\frac{\partial^2}{\partial x \partial y}$, we find the PDE given in Eq. 2.1 where the total division rate is defined by $\beta(x, y, t) \coloneqq \int_0^x \tilde{\beta}(x, y, z, t) \mathrm{d}z$. For the boundary condition at $y = 0$, we take the derivative $\partial / \partial x$ and set $y \to 0^+$ to find

$$g(x, y = 0, t) n(x, y = 0, t) = 2 \int_x^\infty \mathrm{d}x' \int_0^{x'} \mathrm{d}y' \, \tilde{\beta}(x', y', z = x, t) n(x', y', t). \tag{2.3}$$

The other boundary condition defined by construction is $n(x, x, t) = 0$.

In the special restricted case of symmetric cell division, $\tilde{\beta}(x, y, z, t) = \beta(x, y, t) \delta(z - x/2)$, and boundary condition of the adder-sizer model reduces to

$$g(x, y = 0, t) n(x, y = 0, t) = 4 \int_0^{2x} \beta(2x, y', t) n(2x, y', t) \mathrm{d}y'. \tag{2.4}$$

The above derivation provides an explicit boundary condition representing newly born cells that may be asymmetric in birth size. Quantities such as the total cell population $N(t)$ and the mean total biomass $M(t)$ (the total volume over all cells) can be easily constructed from the density $n(x, y, t)$:

$$N(t) = \int_0^\infty \mathrm{d}x \int_0^x \mathrm{d}y \, n(x, y, t), \quad M(t) = \int_0^\infty \mathrm{d}x \int_0^x \mathrm{d}y \, x n(x, y, t). \tag{2.5}$$

Higher moments of the total volume can also be analogously defined. By applying these operations to Eq. 2.1 and using the boundary condition (Eq. 2.3), we find the dynamics of the total population and biomass

$$\frac{\mathrm{d}N(t)}{\mathrm{d}t} = \int_0^\infty \mathrm{d}x \int_0^x \mathrm{d}y\, \beta(x,y,t) n(x,y,t), \quad \frac{\mathrm{d}M(t)}{\mathrm{d}t} = \int_0^\infty \mathrm{d}x \int_0^x \mathrm{d}y\, g(x,y,t) n(x,y,t). \tag{2.6}$$

Finally, we also define the distribution of division events over the size and added size variables, accumulated over a time T:

$$\rho_{\mathrm{d}}(x,y,T) = \frac{\displaystyle\int_0^T \beta(x,y,t) n(x,y,t) \mathrm{d}t}{\displaystyle\int_0^T \mathrm{d}t \int_0^\infty \mathrm{d}x' \int_0^x \mathrm{d}y'\, \beta(x',y',t) n(x',y',t)}. \tag{2.7}$$

2.1. Division probability and connection to time-sizer model. In general, the birth rate functions $\tilde{\beta}(x,y,z,t)$ and $\beta(x,y,t)$ associated with adder-sizer models can take many forms that make biological sense. However, some classes of $\beta(x,y,t)$ may allow the adder-sizer model to be transformed into the well-known "sizer-timer" structured population model [26]. To illustrate the relationship, we consider a division rate function β which depends explicitly only on age a and see how it could be converted to a function of size and added size.

For a cell born at time t_0, the probability that the cell splits within time $[a, a+\mathrm{d}a]$ is defined by $\gamma(a;\bar{a})\mathrm{d}a$. In the absence of death, to ensure that any single cell will eventually split, $\int_0^\infty \gamma(a;\bar{a})\mathrm{d}a = 1$. Reasonable choices for $\gamma(a;\bar{a})$ are Gamma, lognormal, or normal distributions. Without loss of generality, we propose a simple gamma distribution for $\gamma(a;\bar{a})$:

$$\gamma(a;\bar{a}) = \frac{1}{a\Gamma((\bar{a}/\sigma_a)^2)} \exp\left[-\frac{a\bar{a}}{\sigma_a^2} + \left(\frac{\bar{a}}{\sigma_a}\right)^2 \ln\left(\frac{a\bar{a}}{\sigma_a^2}\right)\right], \tag{2.8}$$

where $\bar{a}$ is the mean division age and σ_a^2 is the variance. This type of distribution can be derived from the sum of independent, exponentially distributed ages.

For determinisitic exponential growth $g = \lambda x$, age a and the parameter $\bar{a}$ can be explicitly expressed in terms of x, y and possibly other fixed parameters:

$$a(x,y) = \frac{1}{\lambda}\ln\left(\frac{x}{x-y}\right), \quad \bar{a}(x,y) = \frac{1}{\lambda}\ln\left(\frac{x-y+\Delta}{x-y}\right), \tag{2.9}$$

in which Δ is the fixed added size parameter that represents the adder mechanism.

With $a(x,y)$ and $\bar{a}(x,y)$ defined in Eqs. 2.9, the division rate function $\beta(x,y)$ can be expressed in terms of x and y by using the splitting probability $\gamma(a(x,y);\bar{a}(x,y))$:

$$\beta(x,y,t) = \frac{\gamma(a(x,y);\bar{a}(x,y))}{1 - \int_0^{a(x,y)} \mathrm{d}a' \gamma(a';\bar{a}(x,y))}. \tag{2.10}$$

Assuming this "hazard function" form of a growth law, cells born at small initial size $x(0) = x_0 = x - y$ take longer time to divide, while cells born with large size split sooner. Using the gamma distribution, we find a division rate of the form

$$\beta(x,y) = \frac{\Gamma\left(\frac{\bar{a}^2(x,y)}{\sigma_a^2}\right)\gamma(a(x,y);\bar{a}(x,y))}{\Gamma\left(\frac{\bar{a}^2(x,y)}{\sigma_a^2}, \frac{a(x,y)\bar{a}(x,y)}{\sigma_a^2}\right)}, \tag{2.11}$$

where $\Gamma(\cdot,\cdot)$ is the upper incomplete gamma function. We plot two examples of the time-independent rate $\beta(x,y)$ in Fig. 2.

With $\beta(x,y,t)$ defined, we still need to construct the full fission rate $\tilde{\beta}$, which we will assume is a product of the overall division rate $\beta(x,y,t)$ and a differential division probability. The simplest model is to assume

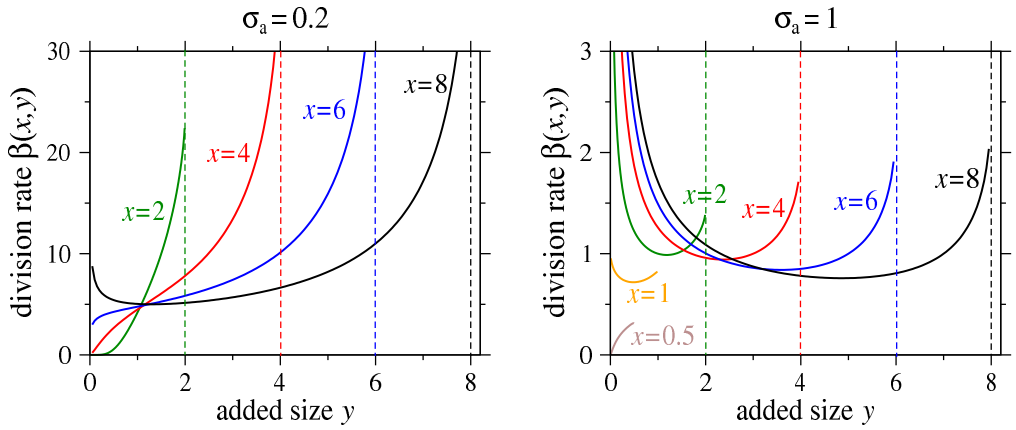


Fig. 2: The size and added-size dependent rate $\beta(x, y)$ constructed using a gamma distribution for the splitting probability γ (Eq. 2.8) and Eq. 2.10. We show projections at fixed values of x. In (a) the parameters are $\sigma_a = 0.2$, while in (b) $\sigma_a = 1$. Note the difference in scale and that $\gamma(a)$ with a higher standard deviation leads to a lower overall cell division rate β. When x is large, $\bar{a}$ defined in 2.9 is small, a nonzero division rate $\beta(x, y \to 0) > 0$ arises indicating that large newborn cells divide quickly to control size across the population. This particular feature arises from our construction of β as a hazard function. Modifying birth rate at small values of y so that $\beta(x, y = 0) \to 0$ will not qualitatively change the predicted densities as long as the birth rate peak persists at small y.

that the differential division probability $h(r)$ is a function of only the ratio r between the size of the daughter cell and that of the mother cell, and independent of the cell size just before division. Thus,

$$\tilde{\beta}(x, y, z, t) = \beta(x, y, t)h(z/x)/x, \tag{2.12}$$

where $r \equiv z/x \in [0, 1]$. The boundary condition (Eq. 2.3) can thus be written in the form

$$g(x, 0, t)n(x, 0, t) = 2\int_x^\infty \mathrm{d}x' \int_0^1 \mathrm{d}s\, \beta(x', sx', t)h(x/x')n(x', sx', t). \tag{2.13}$$

A reasonable model for $h(r = x/x')$ is a lognormal form that is symmetric about $r = 1/2$:

$$h(r) = \frac{h_0(r) + h_0(1 - r)}{Z(\sigma_r, \delta)}, \quad h_0(r) = e^{-\frac{(-\delta+\ln r)^2}{2\sigma_r^2}} e^{-\frac{\ln^2(1-r)}{2\sigma_r^2}}, \tag{2.14}$$

where the parameters δ and σ_r determine the bias and spread of the daughter cell size distribution, and the normalization constant is $Z(\sigma_r, \delta) = \int_0^1 (h_0(r) + h_0(1 - r))\mathrm{d}r$.

2.2. Numerical Implementation and Monte-Carlo Simulations. With the differential birth rate function $\tilde{\beta}$ defined, we can now consider the implementation of numerical solutions to Eqs. 2.1 and 2.3 as well as event-based simulations of the underlying corresponding stochastic process. Since a typical initial condition may not be smooth, a classical solution to Eqs. 2.1 and 2.3 may not exist. Thus, we provide a proof of existence and uniqueness of the weak solution to Eqs. 2.1 and 2.3 in Appendix A. We show convergence of a discrete approximation to our problem, allowing us to confidently numerically approximate the weak solution.

The numerical approximation to the weak solution will be based on an upwind finite difference scheme in which both x and y are discretized with step size h. We define locally averaged functions by

$$f_{i+\frac{1}{2},j+\frac{1}{2}} := \frac{1}{h^2}\int_{ih}^{(i+1)h} \mathrm{d}x \int_{jh}^{(j+1)h} \mathrm{d}y\, f(x, y, t), \tag{2.15}$$

where $f(x,y,t)$ can represent $n(x,y,t)$, $g(x,y,t)$, or $\beta(x,y,t)$. Similarly,

$$\tilde{\beta}_{i+\frac{1}{2},j+\frac{1}{2}}((s+\frac{1}{2})h,t) = h^{-3}\int_{ih}^{(i+1)h} \mathrm{d}x \int_{jh}^{(j+1)h} \mathrm{d}y \int_{kh}^{(k+1)h} \mathrm{d}z\, \tilde{\beta}(x,y,z,t) \tag{2.16}$$

in the domain $i,j \geq 0$ and $j,k < i$. The discretization of the transport equation can be expressed as

$$\begin{aligned} &\frac{n_{i+\frac{1}{2},j+\frac{1}{2}}(t+\Delta t)-n_{i+\frac{1}{2},j+\frac{1}{2}}(t)}{\Delta t} + \frac{g_{i+1,j+\frac{1}{2}}\tilde{n}_{i+1,j+\frac{1}{2}}-g_{i,j}\tilde{n}_{i,j+\frac{1}{2}}}{h} + \frac{g_{i+\frac{1}{2},j+1}\tilde{n}_{i+\frac{1}{2},j+1}-g_{i+\frac{1}{2},j}\tilde{n}_{i+\frac{1}{2},j}}{h} \\ &\qquad = -\beta_{i+\frac{1}{2},j+\frac{1}{2}} n_{i+\frac{1}{2},j+\frac{1}{2}}(t), \end{aligned} \tag{2.17}$$

for $1 \leq i,j \leq L$, where Lh is the maximum size which we take sufficiently large such that $n_{i,j>K}(t=0) = 0, n_{i\leq j} = 0$. We also set $g_{i+\frac{1}{2},i} = 0$ to prevent density flux out of the $y < x$ domain. In Eq. 2.17, $g_{i+1,j+\frac{1}{2}}(t)$ can be taken as $g((i+1)h,(j+\frac{1}{2})h,t)$ while $\tilde{n}_{i+1,j+\frac{1}{2}}(t) = \int_{jh}^{(j+1)h}\mathrm{d}y\, n((i+\frac{1}{2})h,y,t)$ is a finite-volume numerical approximation to $\int_{jh}^{(j+1)h}\mathrm{d}y\, n((i+1)h,y,t)$. The discretized version of the boundary condition (Eq. 2.3) can be expressed as

$$g_{i+\frac{1}{2},0} n_{i+\frac{1}{2},0}(t) = 2h^2 \sum_{k=i+1}^{L}\sum_{j=0}^{k-1} \tilde{\beta}_{k+\frac{1}{2},j+\frac{1}{2}}((i+\frac{1}{2})h,t) n_{k+\frac{1}{2},j+\frac{1}{2}}(t). \tag{2.18}$$

The full explicit discretization scheme for the numerical calculation is provided in Appendix B.

Direct Monte-Carlo simulations of the birth process are also performed and compared with our numerically computed deterministic distributions (see Appendix C). We construct a list of cells and their associated sizes and their sizes at birth. This list is updated at every time step Δt. The cell sizes grow according to $g(x,y,t)$. If a cell divides, the initial sizes of the daughter cells are randomly chosen according to the distribution $h(z/x)$. The daughter cells then replace the mother cell in the list. Simulations of the underlying stochastic process results in, at any given time, a collection of cells, each with a specific size and added size. This collection of cells represents a realization of the population that should be approximated by the distributions that are solutions to Eqs. 2.1 and 2.3.

3. Analysis and Extensions. In this section, we numerically investigate the adder-sizer model and plot various cell population densities and birth event distributions under different parameter regimes. We also show the consistency of numerical solutions of the adder-sizer PDE with results from direct Monte-Carlo simulations of the corresponding stochastic process, which demonstrates that numerical solutions of the linear PDE model for cell population is in agreement with single-cell level stochastic models. After investigating birth rate parameters that can lead to blow-up of population-averaged cell sizes, we extend the basic adder model to include mother-daughter growth rate correlations and processes that measure added size from different points in the cell cycle, *i.e.*, an initation-adder model.

3.1. Cell and division event densities. We evaluated our adder-sizer PDE model by using the division rate given in Eq. 2.10 and first assuming the simple and well-accepted growth function $g(x,y,t) = \lambda x$. Fig. 3 shows the numerical results for the density $\bar{n}(x,y,t) = n(x,y,t)/N(t)$ at successive times $t = 1, 4, 12$, respectively. Stochastic simulations of the underlying process yield cells populations consistent with the deterministic densities derived from the PDE model. In Fig. 4, we compare the cell densities $\bar{n}(x,y,t)$ the division event densities $\rho_{\mathrm{d}}(x,y,T)$ for two different differential division functions $h(r)$. As before, the more asymmetric the division the broader the cell and event densities.

3.2. Cell Volume Explosion. At the single-cell level, a stochastic map model by Kessler and Burov assumed a multiplicative noise and predicted that cell sizes can eventually grow without bound, in agreement with what was experimentally observed for filamentous bacteria [17]. However, stochastic maps of generational cell size do not capture population-level distributions in size or age. In this subsection, we will numerically explore how a possible "blowup" in the population-averaged cell volumes. Within PDE models that describe population distributions, timer and sizer mechanisms have been shown to exhibit blow-up depending on properties of the birth rate $\beta(a,x)$ [1, 7, 16]. Analysis of the conditions on full differential division rate $\tilde{\beta}(x,y,z,t)$ that would

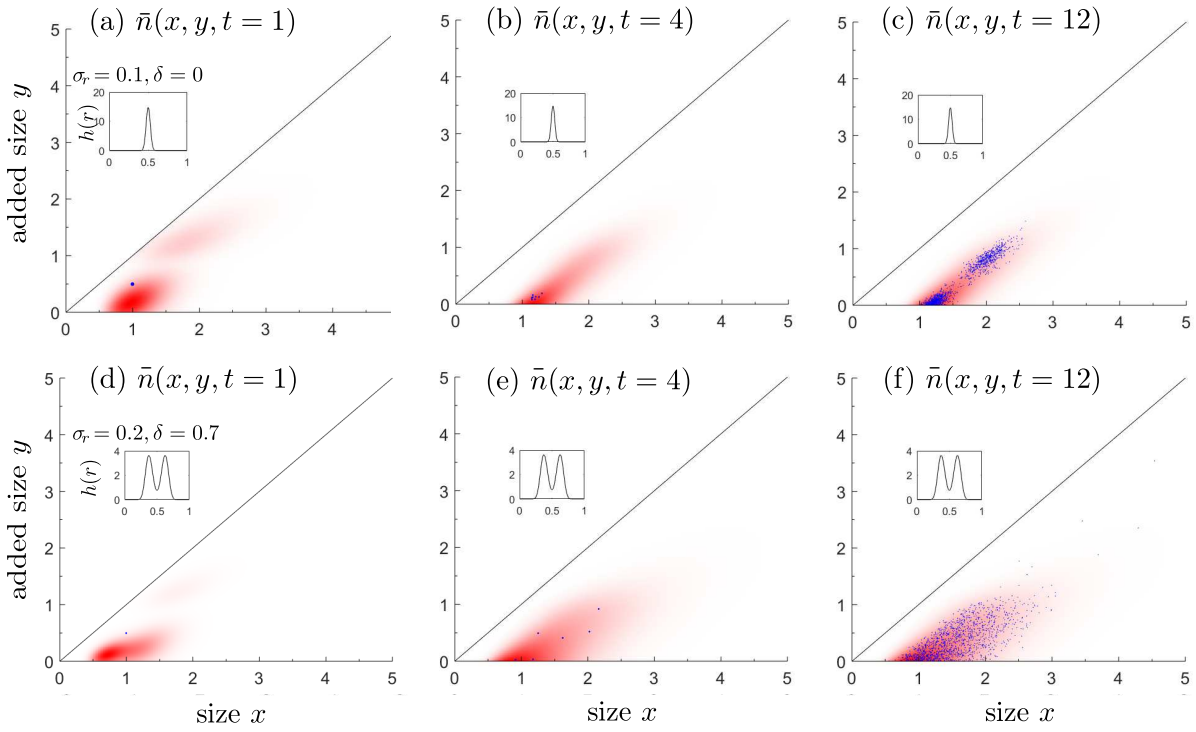


Fig. 3: Numerically computed densities $\bar{n}(x,y,t) = n(x,y,t)/N(t)$ using $g(x,y,t) = \lambda x$ and $\tilde{\beta}(x,y,z,t)$ defined by Eqs. 2.10, 2.8, and 2.14. For all plots, we use $\sigma_a = 0.1$ in $\gamma(a)$ (Eq. 2.8) and rescale size in units of Δ. In (a-c), we use the sharp, single-peaked differential division function $h(r)$ shown in the inset ($\sigma_r = 0.1, \delta = 0$) and plot $\bar{n}(x,y,1), \bar{n}(x,y,4)$, and $\bar{n}(x,y,12)$, respectively. In (d-f), we plot the densities using a broad (in fact, double-peaked) differential division function $h(r)$ with parameters $\sigma_r = 0.2, \delta = 0.7$. In all calculations, we assumed an initial condition corresponding to a single newly born ($y = 0$) cell with size $x = 1$. For more asymmetric cell division in (d-f), the density spreads faster. In these cases, the densities closely approach a steady-state distribution by about $t = 12$. Also shown in each plot are realizations of Monte-Carlo simulations of the discrete process. Individual cells are represented by blue dots which accurately sample the normalized continuous densities $\bar{n}(x,y,t)$.

result in blow-up in the "adder-sizer" PDE model is more involved. Here, we provide only a heuristic argument for sufficient conditions for blow-up.

First, we characterize the shape of the densities in the adder-sizer model. In the analogous McKendrick equation [15] one can investigate the age profile defined by dividing the number density by the total population size. The long term age profile may be stable even when the total population size continuously increases. We take a similar approach here by analyzing $\bar{n}(x,y,t) = n(x,y,t)/N(t)$ where $N(t)$ is given by Eq. 2.5. Writing the adder-sizer PDE in terms of $\bar{n}$, we find

$$\frac{\partial \bar{n}}{\partial t} + \frac{\bar{n}}{N}\frac{\mathrm{d}N}{\mathrm{d}t} + \frac{\partial (g\bar{n})}{\partial x} + \frac{\partial (g\bar{n})}{\partial y} = -\beta \bar{n}. \tag{3.1}$$

Integrating this equation over x, y leads to $\dot{N}/N = \int_0^\infty \mathrm{d}x \int_0^x \mathrm{d}y\, \beta \bar{n}$, which can be substituted into the first term in Eq. 3.1 to yield the nonlinear PDE

$$\frac{\partial \bar{n}}{\partial t} + \frac{\partial (g\bar{n})}{\partial x} + \frac{\partial (g\bar{n})}{\partial y} = -\left(\beta + \int_\Omega \beta \bar{n}\right) \bar{n}. \tag{3.2}$$

A number of standard approaches may be applied to analyze Eq. 3.2. For example, in [15], solutions are attempted by controlling the analogous non-linear integral term. In the adder-sizer problem, we can define

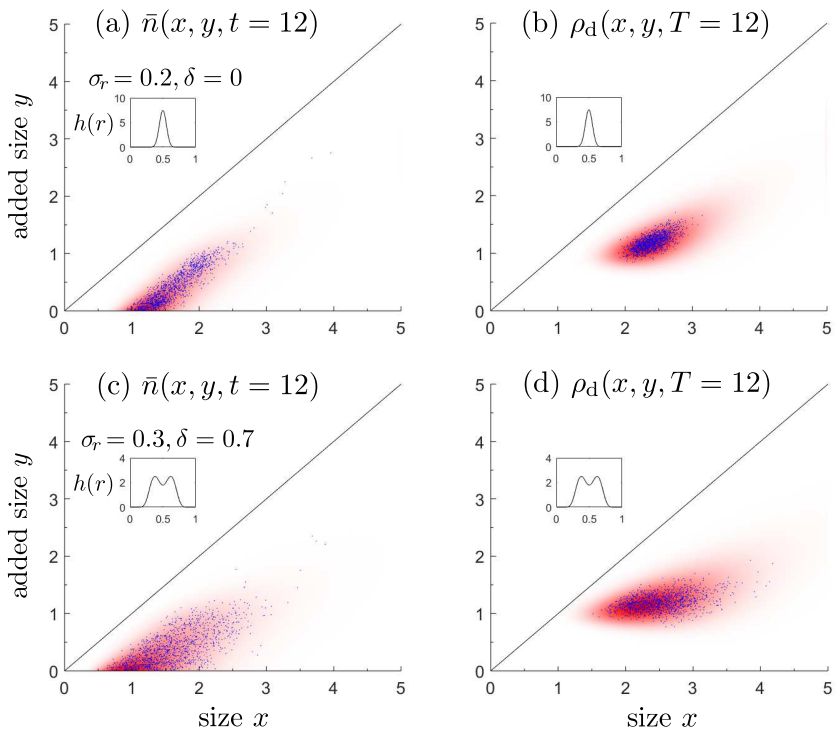


Fig. 4: Comparison of cell densities $\bar{n}(x, y, t)$ and cell division event densities $\rho_{\mathrm{d}}(x, y, T)$ (Eq. 2.7). The standard deviation $\sigma_a = 0.1$ is used in all calculations. In (a) and (b) we plot $\bar{n}(x, y, t = 12)$ and $\rho_{\mathrm{d}}(x, y, T)$ using $\sigma_r = 0.2, \delta = 0$ while in (c) an (d) we used a broader differential division function in which $\sigma_r = 0.3, \delta = 0.7$. Realizations from Monte-Carlo simulations are overlayed. In (b) and (d), divisions are accumulated up to time $T = 12$.

$\langle\beta(t)\rangle = \int_\Omega \beta\bar{n}$ in the above expression to find a self-consistent condition on $\langle\beta(t)\rangle$. One can also assess the steady-state $\bar{n}_{\mathrm{ss}}$ by setting $\frac{\partial\bar{n}_{\mathrm{ss}}}{\partial t} = 0$ and establishing convergence.

One indication of blow-up is a diverging mean cell size $\langle x(t)\rangle = M(t)/N(t)$. By multiplying the Eq. 3.1 by x and integrating (using the boundary condition and symmetry of the $\tilde{\beta}$ distribution) we find

$$\frac{\mathrm{d}\langle x(t)\rangle}{\mathrm{d}t} + \langle\beta(t)\rangle\langle x(t)\rangle = q(t), \tag{3.3}$$

in which $q(t) \coloneqq \int_\Omega g\bar{n}$. If β, g, and $\bar{n} = \bar{n}_{\mathrm{ss}}$ are time-independent and a steady state mean cell size exists, we expect it to obey $\langle x(\infty)\rangle = q(\infty)/\langle\beta(\infty)\rangle$. For the special case of deterministic exponential growth $g(x) = \lambda x$, we can write the time evolution of the mean size as

$$\frac{\mathrm{d}\langle x(t)\rangle}{\mathrm{d}t} = \left[\lambda - \langle\beta(t)\rangle\right]\langle x(t)\rangle, \quad \langle\beta(t)\rangle \equiv \int_0^\infty \mathrm{d}x \int_0^x \mathrm{d}y\, \beta(x, y, t)\bar{n}(x, y, t). \tag{3.4}$$

If $\beta(\infty)$ is bounded above by λ, then we expect blow-up. For $\beta(\infty)$ that is not bounded, as in our example (Eq. 2.10), one cannot determine if blow-up occurs without a more detailed and difficult analysis. Since the precise conditions on β leading to cell volume explosion are difficult to find, we will explore this possible phenomena using numerical experiments. We numerically examine the density $n(x, y, t \to \infty)$ and the mean cell size $\langle x(t)\rangle$ using the $\beta, \tilde{\beta}$ defined in 2.10, 2.8, and 2.14.

In Fig. 5(a) and (b) we plot the marginal distribution $\bar{n}(x, t) \coloneqq \int_x^\infty \mathrm{d}y\, n(x, y, t)/\int_0^\infty \mathrm{d}x \int_x^\infty \mathrm{d}y\, n(x, y, t)$ for different values of the division rate variability σ_a at different times. The associated division rates correspond to those plotted in Fig. 2(a) and (b). In Fig. 5(c) we plot the mean cell sizes $\langle x(t)\rangle = M(t)/N(t)$ corresponding to the distributions in (a) and (b). For sufficiently broad division probabilities $\gamma(a)$ (large σ_a), the division rates β are small, and $\langle x(t)\rangle$ fails to saturate and diverges.

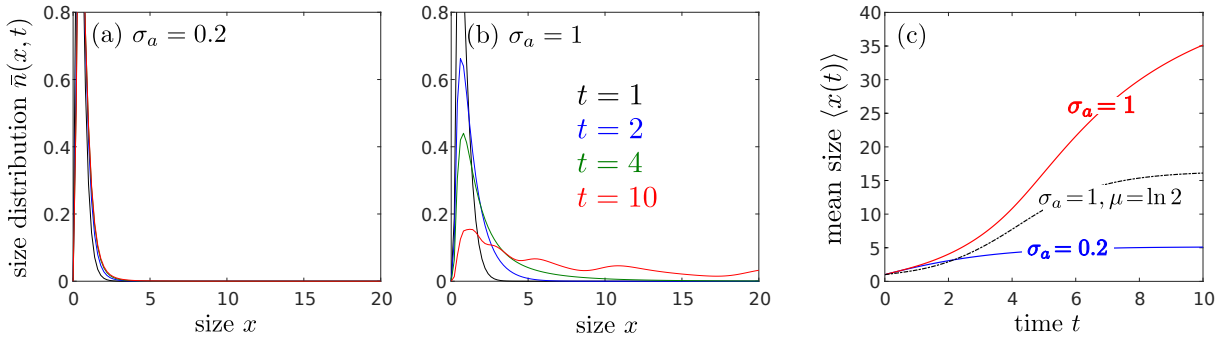


Fig. 5: (a) Size distributions $\bar{n}(x,t)$ for $\sigma_a = 0.2$ at times $t = 1, 2, 4, 10$. (b) $\bar{n}(x, t = 1, 2, 4, 10)$ for $\sigma_a = 1$, $\sigma_r = 0.1$, and $\delta = 0$. (c) The corresponding mean cell sizes $\langle x(t) \rangle$. The curve associated with the $\sigma_a = 0.2$ saturates while the one corresponding to $\sigma_a = 1$ exhibits blow-up. However, the blowup is suppressed if a death term ($\mu = \ln 2$) is included.

3.3. Mother-daughter growth rate correlation. Recent experiments indicate that the growth rate of a mother cell is "remembered" by its daughter cells. For growth rates of the form $g(x, y, t) = \lambda x$, the exponential growth parameter λ between successive generations $i, i+1$ have been proposed to evolve [18, 7]. In [18], fluctuations in λ have been discussed at the single-cell level to explore their effects on the population-averaged growth rate while in [7], changes in growth rates across two consecutive generations are modeled as a Markov process in order to estimate a division rate function β. In this subsection, we first introduce a generalized adder-sizer PDE incorporating variability in λ and then explore the mother-daughter growth rate correlation affects the population dynamics.

A mother-daughter growth rate correlation between two consecutive generations can be described by

$$\lambda_{i+1} = (\lambda_i - \bar{\lambda})R + \bar{\lambda} + \xi, \tag{3.5}$$

where ξ is a random variable, $0 \le R < 1$ is the successive-generation growth rate correlation, and $\bar{\lambda}$ is the mean long-term, or preferred growth rate. Given a growth rate λ_i of a mother cell, Eq. 3.5 describes the predicted growth rate λ_{i+1} of its daughter cells. We assume that the random variable has mean zero and is distributed according to some probability density $P(\xi)$, which vanishes for $\xi \le (1-R)\bar{\lambda}$ to ensure that the growth rates remain positive.

To incorporate the memory of growth rates between successive generations in the adder-sizer PDE model, we extend the cell density in the growth rate variable λ. Thus, $n(x, y, t, \lambda)$ is the density of cells with volume x, added volume y, *and* growth rate λ. The growth function $g(x, y, t, \lambda)$ is now explicitly a function of the growth rate λ. We propose the extended PDE model

$$\begin{cases} \dfrac{\partial n(x,y,t,\lambda)}{\partial t} + \dfrac{\partial (gn)}{\partial x} + \dfrac{\partial (gn)}{\partial y} = -\beta(x,y,t) n(x,y,t,\lambda), \\ g(x,0,t,\lambda) n(x,0,t,\lambda) = 2 \displaystyle\int_0^\infty \mathrm{d}\lambda' \int_x^\infty \mathrm{d}x' \int_0^{x'} \mathrm{d}y\, \tilde{\beta}(x', y, x, t) n(x', y, t, \lambda') P(\xi = \lambda - R\lambda' - (1-R)\bar{\lambda}), \\ \tilde{\beta}(x, y, x', t) = \tilde{\beta}(x, y, x - x', t), \\ n(x, y, 0, \lambda) = n_0(x, y, \lambda), \end{cases} \tag{3.6}$$

A possible symmetric mean zero distribution that vanishes at $-(1-R)\bar{\lambda}$ takes on a log-normal form:

$$P(\xi) \propto \exp\left[-\frac{\ln^2(\xi + (1-R)\bar{\lambda})}{2\sigma_\xi^2} - \frac{\ln^2((1-R)\bar{\lambda} - \xi)}{2\sigma_\xi^2} \right]. \tag{3.7}$$

If we start with one newly born daughter cell at size x_0 and growth rate λ_0, the initial condition in our PDE model would be $n_0(x, y, \lambda) = \delta(x - x_0)\delta(y)\delta(\lambda - \lambda_0)$.

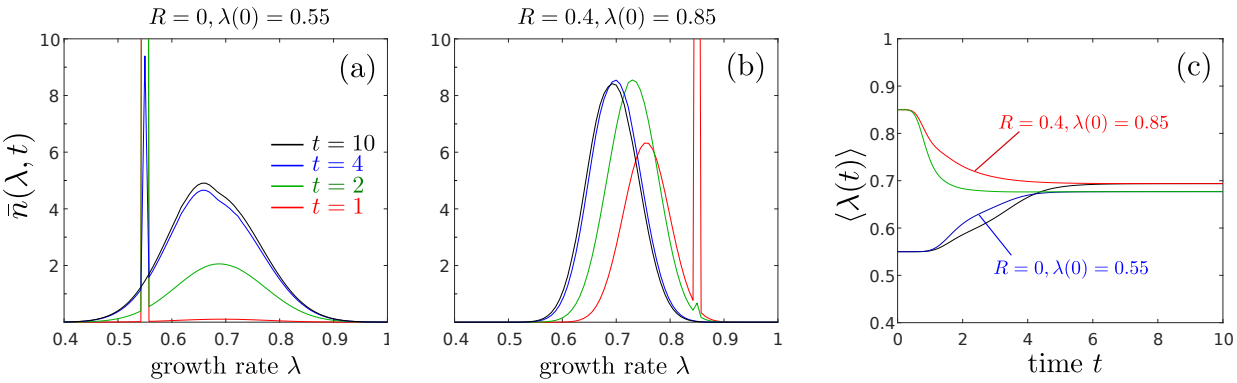


Fig. 6: Population-level evolution of cellular growth rate. Parameters used are $\bar{\lambda} = \ln 2, \sigma_a = 0.2, \sigma_r = 0.1, \delta = 0$. (a-b) The marginalized density $\bar{n}(\lambda, t)$ as a function of growth rate λ for no correlation ($R = 0$) and initial growth rate $\lambda = 0.55$. The peak in the distribution broadens as the mean evolves towards the preferred mean value $\bar{\lambda} = \ln 2$. (c) The evolution of the mean $\langle \lambda(t) \rangle$ for different values of correlation R. Note that the steady-state values $\langle \lambda(\infty) \rangle$ depend on the correlation R.

Numerical solutions of Eqs. 3.6 shown in Fig. 6 indicate that although $\bar{\lambda}$ is the same for two different cases, $R = 0$ and $R = 0.4$, their corresponding mean growth rates $\langle \lambda(t) \rangle$ converge to different values. For larger correlation R, the daughter cells' growth rates do not deviate much from those of their mothers' growth rates. This means that the offspring of faster growing cells tend to grow faster and the offspring of slower growing cells tend to grow slower. Because it takes shorter time for faster cells to divide, they will produce more generations of faster-growing cells, leading to a larger average growth rate defined as

$$\langle \lambda(t) \rangle = \frac{\int_0^\infty \mathrm{d}x \int_0^x \mathrm{d}y \int_0^\infty \mathrm{d}\lambda \ \lambda n(t, x, y, \lambda)}{\int_0^\infty \mathrm{d}x \int_0^x \mathrm{d}y \int_0^\infty \mathrm{d}\lambda n(t, x, y, \lambda)}. \tag{3.8}$$

On the other hand, for a fixed mother growth rate λ_i, smaller correlations R lead to mean daughter cell growth rates $\langle \lambda_{i+1} \rangle$ that are closer to $\bar{\lambda}$. Since cells with growth rates less than $\bar{\lambda}$ will live longer before division, these cells persist in the population longer than those with larger λ, pushing the average growth rate $\langle \lambda(t) \rangle$ to values smaller than $\bar{\lambda}$. Fig. 6(c) explicitly shows that when $R = 0$, the mean growth rate approaches a value smaller than $\bar{\lambda} = \ln 2$.

3.4. Initiation-Adder Model. Recent experiments suggest a new type of adder mechanism for bacterial cell size control [25]. Rather than a fixed volume added between birth and division as the primary control parameter, new experimental evidence suggests that the control parameter in *E. coli* is the added volume between successive initiations of DNA replication. Initiation occurs when the *ori* sites in a cell's genome are separated, leading to DNA replication and segregation. The number of *ori* sites depend on cell type and species, typically one in prokaryotic cells and more than one in eukaryotic cells. The initiation-adder model assumes that a cell's volume per initiation site (the *ori* site in the genome) tends to add a fixed volume between two consecutive initiations.

If the number of *ori* sites in a cell is q, initiation increases the number to $2q$. Immediately after division and DNA separation, the number of *ori*s decreases back to q in each daughter cell.

In this subsection, we generalize the adder PDE model to describe this new initiation-adder mechanism. We classify all cells into two subpopulations: cells that have not yet undergone initiation and cells that have initiated DNA replication but that have not yet divided. We define $n_1(x, y, t)\mathrm{d}x\mathrm{d}y$ as the expected number of pre-initiation cells in with volume in $[x, x+\mathrm{d}x]$ and with added volume $y < x$ in $[y, y+\mathrm{d}y]$. Mean post-initiation cell numbers with volume in $[x, x+\mathrm{d}x]$ and added volume in $[y, y+\mathrm{d}y]$ are described by $n_2(x, y, t)\mathrm{d}x\mathrm{d}y$. In the general initiation-adder process, when a pre-initiation cell commences DNA replication (initiates) can depend on the volume or added volume. Thus, we describe transitions from a pre-initiation cell transitions into a post-initiation cell by the rate $k_\mathrm{i}(x, y, t)$. After initiation, the number of *ori* sites doubles and the added volume is reset to zero in the newly formed post-initiation cell. In analogy with the differential division rate in Eq. 2.1,

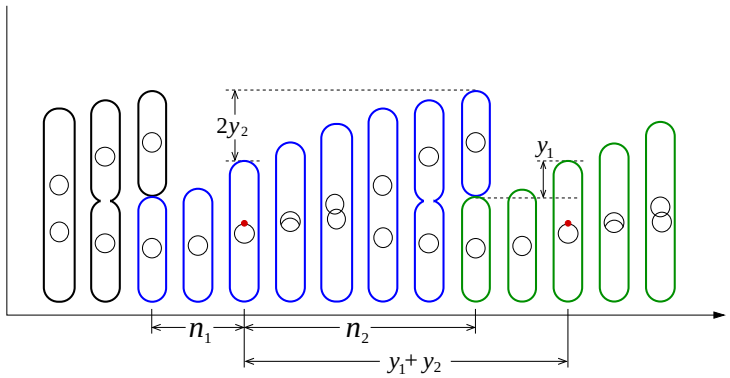


Fig. 7: Schematic for the initiation adder process. DNA replication is initiated (indicated by the red dot) before copied DNA is segregated and cell division. In this example, $q = 1$ and y_2 is and added volume per origination site for two origination sites. The density of cells with $q = 1$ copy of DNA (before DNA replication initiation) is denoted $n_1(x, y, t)$ while the density of cells post-initiation is denoted $n_2(x, y, t)$, where y denotes the volume added after initiation. The factor that controls $y_1 + y_2$ in the initiation-adder model is the volume Δ added between successive initiation events, rather than between successive cell divisions. Thus, the controlled variable (added volume in this case) spans the pre-initiation and post-initiation states.

we define $\beta(x, y, t)$ as the rate of division of post-initiation cells. Under a general asymmetric division event, we assume that the added volume is divided proportionally to the volume of the daughter cells, *i.e.*, if the mother cell's volume is x with added volume y since initiation, and if one daughter cell's volume is $z < x$ and the other daughter cell's volume is $x - z$, the added volume since division for the first daughter will be set to yz/x while the added volume for the second daughter will be $y(x - z)/x$. The resulting PDE model now involves two coupled densities n_1 and n_2:

$$
\begin{aligned}
&\frac{\partial n_1(x,y,t)}{\partial t} + \frac{\partial [g_1 n_1]}{\partial x} + \frac{\partial [g_1 n_1]}{\partial y} = -k_{\rm i}(x,y,t) n_1 + 2\int_x^\infty \frac{z}{x} n_2(z, yz/x, t)\tilde{\beta}(z, x, yz/x, t)\mathrm{d}z,\\
&\frac{\partial n_2(x,y,t)}{\partial t} + \frac{\partial [g_2 n_2]}{\partial x} + \frac{\partial [g_2 n_2]}{\partial y} = -\beta(x,y,t) n_2,\\
&\qquad n_1(x,0,t) = 0, \quad g_2 n_2(x,0,t) = \int_0^x k_{\rm i}(x,y,t) n_1(x,y,t)\mathrm{d}y,\\
&\qquad\qquad \beta(x,y,t) = \int_0^x \tilde{\beta}(x,z,y,t)\mathrm{d}z,
\end{aligned}
\tag{3.9}
$$

in which we have allowed for different growth rates in the different cell phases. Both n_1 and n_2 are defined in the domain $\{\mathbb{R}^{+2} \cap \{y < x\}\} \times \mathbb{R}^+$. These coupled PDEs are different from the PDE associated with the standard "division-adder" described in Eqs. 2.1 and 2.3. Here, the added volume is reset to zero not after division, but after initiation.

In [30], a strong size control acting on initiation initiation was proposed where all cells will have inititated DNA replication before reaching some fixed volume $x_{\rm i}$. This hypothesis can be implemented in our initiation-adder model by setting $k_{\rm i}(x \to x_{\rm i}, y, t) \to \infty$. The probability that a cell born at time t_0 has not yet initiated, $e^{-\int_{t_0}^t k_{\rm i}(x(s),y(s),s)\mathrm{d}s}$, always vanishes for all (t_0, x_{t_0}, y_{t_0}) before some finite time t and $x(t) < x_{\rm i}$. Thus, $n_2(x, 0, t)$ is nonzero only in $[0, x_{\rm i}]$ for all t. If there exists a constant τ_0 such that $\lim_{\tau\to\tau_0} e^{-\int_{t_0}^{t_0+\tau} k_{\rm i}(x(s),y(s),s)\mathrm{d}s} = 0$ for all t_0, then the largest volume that any cell can attain will be $e^{\lambda\tau_0} x_{\rm i}$, leading to strict size control and no blowup.

Fig. 8 shows numerical solutions to Eq. 3.9 using the same birth rate function as that used in Fig. 3(d-f). Note that due to cell size control affecting the pre-initiation stage, initial daughter cell sizes stay small at initiation and $n_1(x, y, t)$ is more peaked near $y \approx x$.

If one takes $k_{\rm i}$ sufficiently large, both daughter cells will nearly instantly initiate DNA replication after division. We have checked numerically that for constant $k_{\rm i} = 10^3$, the densities $n_1(x, y, t)$ are negligible while $n_2(x, y, t)$ approaches the density of the division adder shown in Fig. 3 (for the same differential division functions

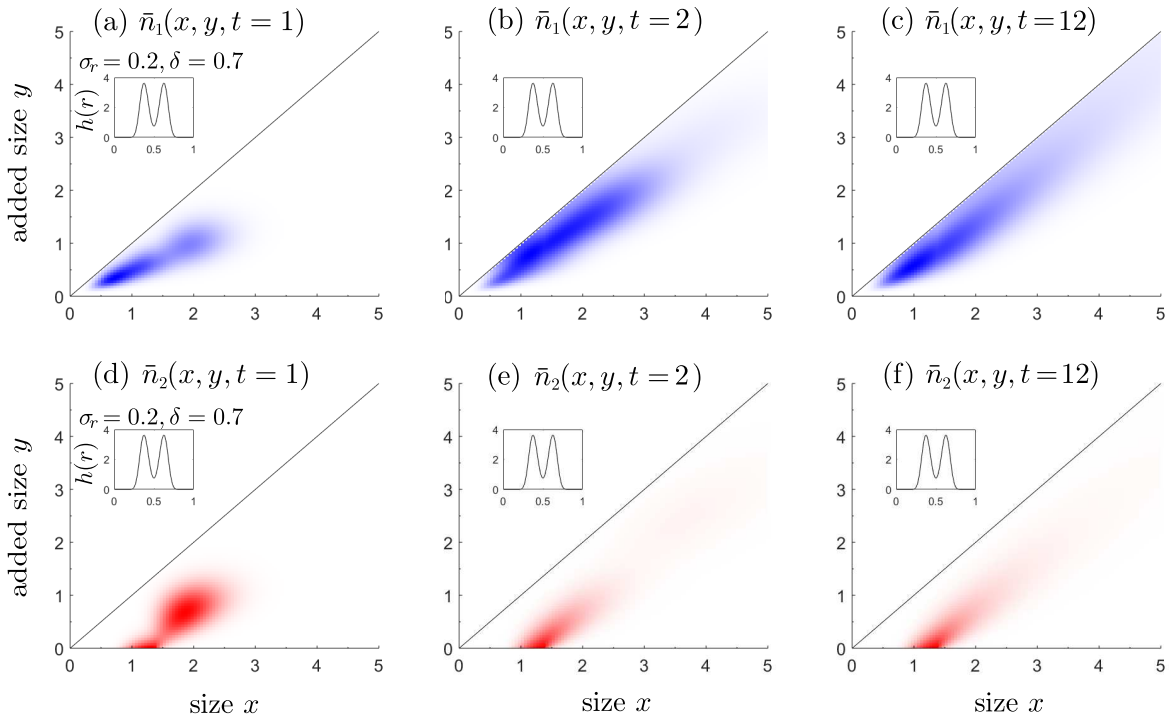


Fig. 8: Normalized densities of pre-initiation cell populations $\bar{n}_1$ and post-initiation cell populations $\bar{n}_2$ for at various fixed times $t = 1, 2, 12$. Here, we used $k_i(x) = p(x)/\left[1 - \int_0^x p(x')\mathrm{d}x'\right]$ with $p(x) \sim \mathcal{N}(1, 0.1)$ and the same $\tilde{\beta}(x, y, z, t)$ as that used in Fig. 3(d-f). (a-c) shows the normalized densities $\bar{n}_1(x, y, t) \equiv n_1(x, y, t)/N(t)$ where $N(t) = \int \mathrm{d}y \int \mathrm{d}x(n_1 + n_2)$. (d-f) shows the normalized post-initiation density $\bar{n}_2(x, y, t)$. For the k_i used in this example, the pre-initiation densities span larger volume and added volumes. The densities are indistinguishable from those at steady state after about $t = 2$.

$\tilde{\beta}$). Thus, the initiation adder model converges to the standard division adder model when $k_i \to \infty$. This can be seen from the first of Eqs. 3.9 where n_1 can be neglected and is dominated by the two terms on the right-hand-side. Substituting $k_i(x, y, t)n_1 \approx 2\int_x^\infty \frac{\mathrm{d}z}{x} n_2(z, yz/x, t)$ into the integral terms in the second equation, we find Eq. 2.1 for $n_2(x, y, t)$.

4. Summary and Conclusions. In this paper, we used PDE models to describe population dynamical behavior under the adder division mechanism. Under certain conditions, this PDE for the adder mechanism can also be converted to the well-known size- and age-structured PDE. In the absence of death, we motivated models for the differential birth rate function $\tilde{\beta}(x, y, z, t)$ that are consistent with normalized division probabilities In Appendix A we showed existence and uniqueness of a weak solution to the PDE model within a time interval $[0, T]$ during which the solution's support can be bounded. One can prove similar results when both time and space are unbounded as this problem is related to other first order PDE models that have been studied in more detail.

With a weak solution justified, we explored the "adder-sizer" PDE via numerical experiments and Monte-Carlo simulations of the underlying stochastic process. Our results show that event-based Monte-Carlo simulations of the discrete process generate sample configurations. The observed configurations are are consistent with samples from the cell densities numerically computed from our PDE model.

When broader differential division rates are used (when cell division is more asymmetric), we find, under the same initial conditions, a broader cell density $n(x, y, t)$ and a broader event density $\rho_D(x, y, T)$. We also demonstrate numerically, the divergence of the mean cell size $\langle x(t)\rangle = M(t)/N(t)$. We showed that division probabilities that are broader in the age or added size (and smaller in magnitude) more likely lead to mean cell sizes that explode with time.

We then incorporated growth rate correlation between cells of successive generations [17] into our "adder-sizer" PDE model. By extending the dimension of the density function to include growth rates and allowing for

variability in growth rate as new cells are born, we developed a PDE model that incorporated the stochastic nature of growth rate inheritance and that describes evolution of the growth rate distribution of cells. We found that the steady-state value of the mean growth rate depends on the correlation of growth rates between mother and daughter cells. This dependence arises from a subtle interaction between the shape of the growth rate distribution and the distribution of variations in the growth rate from one generation to the next.

Finally, we proposed a coupled partial integro-differential equation (PIDE) to model two-phase cell population dynamics under a new initiation-adder mechanism suggested by recent experimental results. In the limit that the initiation rate k_{i} of DNA replication is significantly faster than all other time scales in the problem, the numerical solutions of the initiation adder model (Eq. 3.9) converge to those of division adder model (Eqs. 2.1 and 2.3). Under proper assumptions that come from experimental findings, we found that the initiation adder would also lead to effective cell size control [30].

There are new cellular processes and size control mechanisms that have been recently discovered and that can be mathematically modeled. Thus, there is likely general mathematical topics that remain to be explored within PDE and PIDE models of structured populations. For example, a recent experimental study indicates that an adder mechanism may be the result of several consecutive processes in the cell division cycle, suggesting that a much more complicated coupled system of PDEs/PIDEs would be required.

Acknowledgments. This work was supported in part by grants from the NSF (DMS-1814364), the National Institutes of Health (R01HL146552) and the Army Research Office (W911NF-18-1-0345).

Appendix A. Existence and uniqueness of a weak solution for the adder-sizer model.

In this section we show the existence and uniqueness of the solution to the "adder-sizer" model PDE. The full problem is defined as

$$
\begin{cases}
\dfrac{\partial n}{\partial t} + \dfrac{\partial (ng)}{\partial x} + \dfrac{\partial (ng)}{\partial y} = -\beta(x,y,t) n(x,y,t), \\
g(x,0,t) n(x,0,t) = 2 \displaystyle\int_x^\infty \mathrm{d}x' \int_0^{x'} \mathrm{d}y\, \tilde{\beta}(x',y,x,t) n(x',y,t), \\
\beta(x,y,t) \coloneqq \displaystyle\int_0^x \tilde{\beta}(x,y,z,t) \mathrm{d}z, \\
\tilde{\beta}(x,y,z',t) = \tilde{\beta}(x,y,z-z',t),\ \tilde{\beta}(x,y,0,t) = 0,\ n(x,x,t) = 0, \\
n(x,y,t=0) \coloneqq n_0(x,y).
\end{cases}
\tag{A.1}
$$

where the independent variables $(x,y,t) \in \mathbb{R}^2 \cap \{y < x\} \times \mathbb{R}^+$.

First, we assume that

$$
\begin{aligned}
0 < g_{\min} \leq g \in & \mathbf{C}^1(\{(\mathbb{R}^+)^2 \cap \{y \leq x\}\} \times \mathbb{R}^+), \\
n_0(x,y) \in & \mathbf{L}^1 \cap \mathbf{L}^\infty \cap \mathbf{C}^1(\mathbb{R}^+ \cap \{y < x\}), \\
0 \leq \tilde{\beta} \in & \mathbf{L}^\infty \cap \mathbf{L}^1 \cap \mathbf{C}^1(\{(\mathbb{R}^+)^3 \cap \{y < x, z < x\}\} \times \mathbb{R}^+), \\
\beta(x,y,t) \in & \mathbf{L}^\infty \cap \mathbf{L}^1 \cap \mathbf{C}^1(\{(\mathbb{R}^+)^2 \cap \{y \leq x\}\} \times \mathbb{R}^+),
\end{aligned}
\tag{A.2}
$$

and nondimensionalize the size and added size by Δ, the added size parameter defined in Eq. 2.9. We also impose an additional assumption on g:

$$
|g(x,y,t)| < K(t+x+1), \quad K < \infty. \tag{A.3}
$$

We also assume the initial distribution $n_0(x,y)$ is compactly supported in $(0,\Omega) \times [0,\Omega), \Omega < \infty$. From this assumption and A.3, the closure of $n(x,y,T)$'s support is compact for any finite time T since $n \neq 0$ only when $y < x$ and $x(s) \leq Ce^{Ks} - (1+T)$ from Grönwall's Inequality, where $C < 1 + T + \Omega$ is given by the initial condition. At any finite time T, the support of $n(x,y,T)$ is bounded and we assume it is contained in $[0,\Omega(T)) \times [0,\Omega(T))$. Furthermore, by setting $g, \beta, \tilde{\beta} = 0$ at the given time T when (x,y) is out of the support of n, we can assume the closure of $g, \beta, \tilde{\beta}$'s support to be compact. One can generalize the definition of the weak solution n to $[(\mathbb{R}^+)^2 \cap \{y < x\}] \times [0,\infty)$ as in [22].

Definition A.1 Given time $T < \infty$ and assuming A.2, for a function $n \in \mathbf{L}^1((([0,\Omega(T)])^2 \cap \{y < x\}) \times [0,T]), \Omega(T) < \infty$ with $n(x,y,t) \neq 0$ in $[0,\Omega(T)) \times [0,\Omega(T)), y < x, t \in [0,T]$, n is said to satisfy the adder-sizer PDE in the weak sense in time $[0,T]$, if

$$\begin{aligned} -\int_0^T \mathrm{d}t \int_0^\infty \mathrm{d}x \int_0^x \mathrm{d}y\, n(x,y,t) \left[\frac{\partial \Psi}{\partial t} + g(x,y,t)\frac{\partial \Psi}{\partial x} + g(x,y,t)\frac{\partial \Psi}{\partial y} - \beta(x,y,t)\Psi(x,y,t)\right] \\ = \int_0^\infty \mathrm{d}x \int_0^x \mathrm{d}y\, n_0(x,y)\Psi_0(x,y) + \int_0^T \mathrm{d}t \int_0^\infty \mathrm{d}x\, \Psi(x,0,t) n(x,0,t) g(x,0,t) \end{aligned} \tag{A.4}$$

holds for all test functions $\Psi \in \mathbf{C}^1((([0,\Omega(T)])^2 \cap \{y \leq x\}) \times [0,T])$ satisfying $\Psi(x,y,T) \equiv 0, \Psi(\Omega(T),y,t) = 0$ and $\Psi(x,x,t) = 0$, where we set $g, \tilde{\beta}, \beta = 0$ for $x \geq \Omega(T), x \leq y$ or $x \leq z$. Upon using the boundary condition in A.1, the right-hand-side becomes

$$\int_0^\infty \mathrm{d}x \int_0^x \mathrm{d}y\, n_0(x,y)\Psi_0(x,y) + 2\int_0^T \mathrm{d}t \int_0^\infty \mathrm{d}x \int_0^x \mathrm{d}y \int_0^x \mathrm{d}z\, \Psi(z,0,t)\tilde{\beta}(x,y,z,t) n(x,y,t).$$

Note that if $n \in \mathbf{C}^1(((\mathbb{R}^+)^2 \cap \{y < x\}) \times \mathbb{R}^+)$ is a classical solution to the PDE (Eq. A.1), then it must also satisfy Eq. A.4 in any time interval $[0,T]$. We refer to [22] for a proof of the existence and uniqueness of a weak solution of a related, simpler renewal equation. However, our adder-sizer PDE is more complicated. The proof of uniqueness requires very different techniques from the sizer PDE; yet the proof of existence is similar to the proof in [22].

A.1. Uniqueness. First, we prove uniqueness of the solution to A.4. Assume there are two weak solutions $n^{(0)}$ and $n^{(1)}$ for the adder-sizer PDE satisfying A.4 with the same initial condition $n_0^{(0)}(x,y) = n_0^{(1)}(x,y)$. Taking the difference between using these purported solutions, we obtain

$$\begin{aligned} -\int_0^T \mathrm{d}t \int_0^\infty \mathrm{d}x \int_0^x \mathrm{d}y\, \Delta n(x,y,t) \left[\frac{\partial \Psi}{\partial t} + g(x,y,t)\frac{\partial \Psi}{\partial x} + g(x,y,t)\frac{\partial \Psi}{\partial y} - \beta(x,y,t)\Psi(x,y,t)\right] \\ = 2\int_0^T \mathrm{d}t \int_0^\infty \mathrm{d}x \int_0^x \mathrm{d}y \int_0^x \mathrm{d}z\, \Psi(z,0,t)\tilde{\beta}(x,y,z,t)\Delta n(x,y,t), \end{aligned} \tag{A.5}$$

where $\Delta n = n^{(1)} - n^{(0)}$.

A.1.1. Adjoint Problem. We consider the adjoint problem for Ψ in the given time interval $[0,T]$ and with a source term $S(x,y,t)$:

$$\begin{aligned} \frac{\partial \Psi}{\partial t} + g(x,y,t)\frac{\partial \Psi}{\partial x} + g(x,y,t)\frac{\partial \Psi}{\partial x} - \beta(x,y,t)\Psi(x,y,t) = -2\int_0^x \Psi(z,0,t)\tilde{\beta}(x,y,z,t)\mathrm{d}z - S(x,y,t), \quad 0 \leq y < x \\ \Psi(x,y,T) = 0,\ \Psi(\Omega(T),y,t) = 0,\ \Psi(x,x,t) = 0. \end{aligned} \tag{A.6}$$

Theorem A.1 Assume A.2, and $S \in \mathbf{C}^1([0,\Omega(T)]^2 \times [0,T]), S(\Omega(T),y,t) = 0$, and $S = 0$ when $x \leq y$. Then there exists a unique $\mathbf{C}^1$ solution to the adjoint problem.

Proof. We can transform the above equation into an ODE along the characteristic line and use contraction mapping, which is a standard practice in functional analysis to prove existence and uniqueness of the solution to a PDE problem. On the left-hand-side of Eq. A.6, we apply the characteristic line method. Setting $X(c,t) = (x(c,t), y(c,t))$ on the characteristic lines leads to

$$\begin{cases} \dfrac{\partial X(c,s)}{\partial s} = (g(x,y,s), g(x,y,s)), \quad t \leq s \leq T, \\ X(c,t) = (x_t, y_t), \quad 0 \leq y_t < x_t, x_t - y_t = c. \end{cases}$$

Since we have $x(s) - y(s) = x_t - y_t$, the above equation can be simplified to

$$\frac{\partial X(c,s)}{\partial s} = \tilde{g}(X(c,s),s),\ x(c,t) = x_t,\ y(c,t) = x_t - c$$

where $\tilde{g}(X(c,s),s) = (g(x(c,s), x(c,s)-c,s),\ g(x(c,s), x(c,s)-c,s))$. Once c is fixed and x_t is given, the above equation becomes an ordinary differential equation. Given x_t, we define

$$\begin{cases} \tilde{\Psi}(c,s) \coloneqq \Psi(X(c,s),s)e^{-\int_t^s \beta(X(c,v),v)dv}, \\ U(c,z,s) \coloneqq 2\tilde{\beta}(X(c,s),z,s)e^{-\int_t^s \beta(X(c,v),v)dv},\ \tilde{S}(c,s) \coloneqq S(X(c,s),s)e^{-\int_t^s \beta(X(c,v),v)dv}. \end{cases}$$

Thus, along the characteristic line we can write A.6 as

$$\frac{\partial}{\partial s}\tilde{\Psi}(c,s) = -\int_0^{x(c,s)} \Psi(z,0,s)U(c,z,s)\mathrm{d}z - \tilde{S}(c,s). \tag{A.7}$$

Since $\tilde{\Psi}(c,T) = 0$ and $\tilde{\Psi}(c,t) = \Psi(x_t, x_t - c, t)$,

$$\Psi(x_t, x_t - c, t) = \int_t^T \tilde{S}(c,s)\mathrm{d}s + \int_t^T \mathrm{d}s \int_0^{x(c,s)} \mathrm{d}z\, \Psi(z,0,s)U(c,z,s), \quad 0 < c \le x_t. \tag{A.8}$$

We can see that if $x \le y$ or $x_t \ge \Omega(T)$, $\Psi(t, x_t, x_t - c) = \Psi(t,x,x) = 0$ since $U, \tilde{S} = 0$ for $c \le 0$ or $x_t > \Omega(T)$. Using $c = x_t$, Eq. A.8 becomes

$$\Psi(x_t, 0, t) = \int_t^T \tilde{S}(x_t,s)\mathrm{d}s + \int_t^T \mathrm{d}s \int_0^{x(x_t,s)} \mathrm{d}z\, \Psi(z,0,s)U(x_t,z,s). \tag{A.9}$$

From condition A.3 we obtain $x(s) \le (x_t+1+T)e^{K(s-t)} - (1+T)$. From condition A.3, we define $\tilde{B} = 2\|\tilde{\beta}\|_\infty < \infty$. Next, we choose $s = \max\{T - \frac{1}{K}\ln(1+\frac{1}{2\tilde{B}(1+T)}), T - \frac{1}{K}\ln 2, T-1\}$ such that $e^{K(T-t)} \le 1 + \frac{1}{2\tilde{B}(1+T)}$, $s \le t \le T$, and choose x_s small enough such that $x_s < \min\{1, \frac{1}{8\tilde{B}(T-s)}\}$. We denote a mapping T defined on the functional space as

$$T(\Psi)(x_t,0,t) = \int_t^T \tilde{S}(x_t,s)\mathrm{d}s + \int_t^T \mathrm{d}s \int_0^{x(s,x_t)} \mathrm{d}z\, \Psi(z,0,s)U(x_t,z,s), \quad t \in [s,T], x_t \in [0, x_s].$$

It is easy to verify that T is a contraction mapping for $\Psi(x_t,0,t)$ and thus there exists a unique solution Ψ_0 satisfying A.6 in D_0 defined as $D_0 = \{(x,t) | s \le t \le T, 0 \le x \le x(x_s,t)\}$. We then let $x_s^1 > x_s$ and define $D_1 = \{(x,t) | s \le t \le T, 0 \le x \le x(x_s^1, t)\}$ such that the difference of the area between regions D_1 and D_0 is less than $\tilde{B}^{-1}$. Next, define a second mapping T_1 by

$$\begin{cases} T_1(\Psi)(x_t,0,t) = \displaystyle\int_t^T \mathrm{d}s \int_{x(x_s,s)}^{x(x_t,s)} \mathrm{d}z\, \Psi(z,0,s)U(x_t,z,s) + I(x_s,t), \quad t \in [s,T],\ x_t \in [x(t,x_s), x_s^1], \\ I(x_s,t) = \displaystyle\int_t^T \mathrm{d}s\, \tilde{S}(x_t,s) + \int_t^T \mathrm{d}s \int_0^{x(x_s,s)} \mathrm{d}z\ \Psi_0(z,0,s)U(x_t,z,s). \end{cases}$$

T_1 is also a contraction mapping and we can obtain a Ψ_1 on D_1 such that $T(\Psi_1) = \Psi_1$. Denote

$$\Psi(x,0,t) = \begin{cases} \Psi_0(x,0,t),\ (x,t) \in D_0, \\ \Psi_1(x,0,t),\ (x,t) \in D_1, \end{cases} \tag{A.10}$$

and it is easy to verify that Ψ is C^1 continuous on $D_0 \cap D_1$ by first proving it is continuous and then taking the partial derivatives, and Ψ satisfy A.6 in the region $D_0 \cup D_1$.

Following the same procedure, we can extend Ψ to satisfy A.6 in the region $t \in [s,T]$. Then, for $[0,s]$, we choose a $\tilde{s}$ close enough to s and use the same strategy by defining T_2 as

$$\text{(A.11)}\qquad \begin{cases} T_2(\Psi)(x_t,0,t)=\displaystyle\int_t^s \mathrm{d}r\,\tilde{S}(x_t,r)+\int_t^s \mathrm{d}r\int_0^{x(x_t,r)}\mathrm{d}z\,\Psi(z,0,r)U(x_t,z,r)+\tilde{I}(t,x_s),\ t\in[\tilde{s},s],\\ \tilde{I}(x_s,t)=\displaystyle\int_s^T \mathrm{d}r\,\tilde{S}(x_t,r)+\int_s^T \mathrm{d}r\int_0^{x(x_t,r)}\mathrm{d}z\,\Psi(z,0,r)U(x_t,z,r) \end{cases}.$$

We finally obtain a unique function Ψ satisfying A.6 in $[0,T]\times[0,\infty)$.

From A.8, the value of Ψ is determined by $\tilde{S},\Psi(x,0,t),U$ and we conclude that there exists a unique $\mathbf{C}^1$ solution for A.6.

A.1.2. Uniqueness of weak solution for the adder-sizer model. From Section A.1.1 we obtain the existence and uniqueness of Ψ of the adjoint problem. Given any time T and $S(x,y,t)\in\mathbf{C}^1(\mathbb{R}^+\times(\mathbb{R}^+)^2)$ satisfying the condition in Theorem A.1, since we can set $g,\beta,\tilde{\beta}$'s support to be compact in $[0,T]$, we can find a unique $\mathbf{C}^1$ continuous Ψ satisfying A.6. By substituting A.6 into A.5, we obtain

$$\text{(A.12)}\qquad \int_0^T \mathrm{d}t\int_0^{\Omega(T)}\mathrm{d}x\int_0^x \mathrm{d}y\,\Delta n(x,y,t)S(x,y,t)=0$$

for any $S(x,y,t)\in\mathbf{C}^1(\mathbb{R}^+\times\mathbb{R}^{+2})$ satisfying $S(x\le y,t)=S(x\ge\Omega(T),y,t)=0$, which implies $n\equiv 0$ a.e. in $y<x\le\Omega(T)$. So at any given time T the weak solution, if exists, is unique.

One can also set the condition for $\tilde{\beta},g$ weaker even when we define the weak solution in unbounded region $[0,\infty)\times(\mathbb{R}^+)^2\cap\{y<x\}$. In [22] such work is done for the renewal equation. We do not discuss this generalization in detail here.

A.2. Existence of the weak solution. We construct a series of functions $\{n_i\}$ with a limit n for this series satisfying A.6 for all test functions Ψ. We use a semi-discrete approximation to discretize the PDE and obtain piecewise solutions. As the mesh size becomes smaller, we expect the piecewise solution to converge to a function n satisfying A.4. The idea of constructing a series of piecewise constant solutions and proving their convergence to a weak solution is similar to that in [22].

A.2.1. Semi-discrete approximation for the PDE. We choose a uniform grid with mesh size $h>0$ fixed in both x and y axis and let time t be continuous. We denote

$$\text{(A.13)}\qquad \begin{aligned} (x_i,y_j)=(ih,jh),(x_{i+\frac12},y_{j+\frac12})&=((i+\frac12)h,(j+\frac12)h),\quad j<i\in\mathbf{N},\\ \beta_{i+\frac12,j+\frac12}(t)&=\frac{1}{h^2}\int_{ih}^{(i+1)h}\mathrm{d}y\int_{jh}^{(j+1)h}\mathrm{d}x\,\beta(x,y,t),\quad j<i\in\mathbf{N},\\ \tilde{\beta}_{i+\frac12,j+\frac12}((s+\frac12)h,t)&=\frac{1}{h^3}\int_{ih}^{(i+1)h}\mathrm{d}z\int_{jh}^{(j+1)h}\mathrm{d}y\int_{sh}^{(s+1)h}\mathrm{d}x\,\tilde{\beta}(x,y,z,t),\quad s\le i,\\ g_{i,j}(t)&=g(ih,jh,t),\quad j<i\in\frac12\mathbf{N}. \end{aligned}$$

Here, $\beta_{i+\frac12,j+\frac12}(t)=h\sum_{s=0}^{i}\tilde{\beta}_{i+\frac12,j+\frac12}((s+\frac12)h,t)$. Given a fixed time T, we wish to find a solution of pointwise function $n^h(t)$, which takes values on the grid points $(x_{i+\frac12},y_{j+\frac12})$. Then n^h can be seen as a vector function. According to our assumption there exists Ω such that the initial value n^0 is nonzero within the region $\{(x,y)|y<x,x<\Omega\}$, and from our previous calculation there exists $\Omega(T)<\infty$ such that n is nonzero within the region $\{(x,y)|y<x,x<\Omega(T)\}$. Eventually, we will set $h(k)=\Omega(T)/k$ and let the mesh size $h\to 0$ by letting $k\to\infty$.

By discretizing Eqs. A.1, we expect the vector function $n^h(t)$ to satisfy the below equations for $t\in[0,T]$ and $0<j<i<L$ (L is the number of discretization grid points along one direction):

(A.14)

$$h^2\frac{\mathrm{d}n_{i+\frac{1}{2},j+\frac{1}{2}}(t)}{\mathrm{d}t}+h(g_{i+1,j+\frac{1}{2}}(t)n_{i+\frac{1}{2},j+\frac{1}{2}}(t)-g_{i,j+\frac{1}{2}}(t)n_{i-\frac{1}{2},j+\frac{1}{2}}(t))$$
$$+h(g_{i+\frac{1}{2},j+1}(t)n_{i+\frac{1}{2},j+\frac{1}{2}}(t)-g_{i+\frac{1}{2},j}(t)n_{i+\frac{1}{2},j-\frac{1}{2}}(t))+h^2\beta_{i+\frac{1}{2},j+\frac{1}{2}}(t)n_{i+\frac{1}{2},j+\frac{1}{2}}(t)=0,\quad 0\le j<i-1$$

$$h^2\frac{\mathrm{d}n_{i+\frac{1}{2},j+\frac{1}{2}}(t)}{\mathrm{d}t}+hg_{i+1,j+\frac{1}{2}}(t)n_{i+1,j+\frac{1}{2}}(t)$$
$$-hg_{i+\frac{1}{2},j}(t)n_{i+\frac{1}{2},j-\frac{1}{2}}(t)+h^2\beta_{i+\frac{1}{2},j+\frac{1}{2}}(t)n_{i+\frac{1}{2},j+\frac{1}{2}}(t)=0,\quad 0\le j=i-1$$

$$g_{i+\frac{1}{2},0}(t)n_{i+\frac{1}{2},-\frac{1}{2}}(t)=2h^2\sum_{\ell=i}^{L-1}\sum_{j=0}^{\ell-1}\tilde{\beta}_{\ell+\frac{1}{2},j+\frac{1}{2}}((i+\frac{1}{2})h,t)n_{\ell+\frac{1}{2},j+\frac{1}{2}}(t),$$

$$n_{i+\frac{1}{2},j+\frac{1}{2}}(0)=\frac{1}{h^2}\int_{x_i}^{x_{i+1}}\mathrm{d}y\int_{y_j}^{y_{j+1}}\mathrm{d}x\,n_0(x,y),\quad n_{i+\frac{1}{2},i+\frac{1}{2}}(t)=0,$$

where we henceforth omit the h superscript in the proof. In the two-dimensional upwind scheme, derivatives in one direction are neglected on neighboring sites in the other direction: $n_{i,j\pm\frac{1}{2}}=n_{i-\frac{1}{2},j\pm\frac{1}{2}},n_{i\pm\frac{1}{2},j}=n_{i\pm\frac{1}{2},j-\frac{1}{2}}$. The boundary condition $n(x,x,t)=0$ is implemented by $n_{i+\frac{1}{2},i+\frac{1}{2}}(t)=0$ for any t and i.

We will obtain a uniform bound irrelevant of h for n. All coefficients in the above ODE equations are $\mathbf{C}^1$ continuous, which means that there exists a unique solution in time $[0,T],T<\infty$.

Theorem A.2 For $t\in[0,T]$ and assuming A.2 holds, we find the bound

$$\sum_{i=1}^{L-1}\sum_{j=0}^{i}|n_{i+\frac{1}{2},j+\frac{1}{2}}(t)|\le e^{Mt}\sum_{i=1}^{L-1}\sum_{j=0}^{i}|n_{i+\frac{1}{2},j+\frac{1}{2}}(0)|, \tag{A.15}$$

where $\tilde{B}=2\|\tilde{\beta}\|_\infty, M=2B-b, B=\|\beta\|_\infty$, and $b=\min_t\min_{i,j}\beta_{i+\frac{1}{2},j+\frac{1}{2}}(t)$. The $\mathbf{L}^\infty$ bound is given by $\|n^h(t)\|_\infty\le\max\{\frac{1}{g_{\min}}\tilde{B}e^{MT}\|n(0)\|_1,\|n^h(0)\|_\infty\}e^{2\tilde{g}'t}$ where $\tilde{g}'$ is the $\mathbf{L}^\infty$ bound of $\partial g/\partial x,\partial g/\partial y$.

Proof For the summation of n over all grid points, we multiply the first equation in A.14 by $\mathrm{sign}(n_{i+\frac{1}{2},j+\frac{1}{2}})$ for each $i,j\le i$,

(A.16)

$$h^2\frac{\mathrm{d}}{\mathrm{d}t}|n_{i+\frac{1}{2},j+\frac{1}{2}}(t)|+hg_{i+1,j+\frac{1}{2}}(t)|n_{i+\frac{1}{2},j+\frac{1}{2}}(t)|+hg_{i+\frac{1}{2},j+1}(t)|n_{i+\frac{1}{2},j+\frac{1}{2}}(t)|+h^2\beta_{i+\frac{1}{2},j+\frac{1}{2}}(t)|n_{i+\frac{1}{2},j+\frac{1}{2}}(t)|\le$$
$$hg_{i,j+\frac{1}{2}}(t)|n_{i-\frac{1}{2},j+\frac{1}{2}}(t)|+hg_{i+\frac{1}{2},j}(t)|n_{i+\frac{1}{2},j-\frac{1}{2}}(t)|$$

By multiplying the second equation in A.14 by $\mathrm{sign}(n_{i+\frac{1}{2},j+\frac{1}{2}})$ for each $i,j\le i$ pair and summing over index $\sum_{i=1}^{L-1}\sum_{j=0}^{i-1}$,

$$h^2\sum_{i=1}^{L-1}\sum_{j=0}^{i-1}|n_{i+\frac{1}{2},j+\frac{1}{2}}(t)|+h\sum_{j=0}^{i-1}g_{L,j+\frac{1}{2}}(t)|n_{L-1+\frac{1}{2},j+\frac{1}{2}}(t)|$$
$$+h^2\sum_{i=1}^{L-1}\sum_{j=0}^{i-1}\beta_{i+\frac{1}{2},j+\frac{1}{2}}(t)|n_{i+\frac{1}{2},j+\frac{1}{2}}(t)|\le h\sum_{i=0}^{L-1}g_{i+\frac{1}{2},0}(t)|n_{i+\frac{1}{2},-\frac{1}{2}}(t)|.$$

We can simplify the above expression to

$$h^2\frac{d}{dt}\sum_{i=1}^{L-1}\sum_{j=0}^{i-1}|n_{i+\frac{1}{2},j+\frac{1}{2}}(t)|+h^2\sum_{i=1}^{L-1}\sum_{j=0}^{i-1}\beta_{i+\frac{1}{2},j+\frac{1}{2}}|n_{i+\frac{1}{2},j+\frac{1}{2}}(t)|$$

$$\leq 2h^3 \sum_{i=0}^{L-1} \Big| \sum_{\ell=i}^{L-1} \sum_{j=0}^{\ell-1} \tilde{\beta}_{\ell+\frac{1}{2},j+\frac{1}{2}}((i+1/2)h,t) n_{\ell+\frac{1}{2},j+\frac{1}{2}}(t) \Big|$$
$$\leq 2h^2 \sum_{\ell=1}^{L-1} \sum_{j=0}^{\ell-1} |\beta_{\ell+\frac{1}{2},j+\frac{1}{2}}(t)||n_{\ell+\frac{1}{2},j+\frac{1}{2}}(t)|.$$

We then have

$$\frac{\mathrm{d}}{\mathrm{d}t} \sum_{i=1}^{L-1} \sum_{j=0}^{i-1} |n_{i+\frac{1}{2},j+\frac{1}{2}}(t)| \leq (2B-b) \sum_{i=1}^{L-1} \sum_{j=0}^{i-1} |n_{i+\frac{1}{2},j+\frac{1}{2}}(t)|,$$

which yields

$$\sum_{i=1}^{L-1} \sum_{j=0}^{i-1} |n_{i+\frac{1}{2},j+\frac{1}{2}}(t)| \leq e^{Mt} \sum_{i=1}^{L-1} \sum_{j=0}^{i-1} |n_{i+\frac{1}{2},j+\frac{1}{2}}(0)|. \tag{A.17}$$

A.17 states that the l^1 norm of all the values on the grid points are uniformly bounded and independent of h. Next, we estimate the $\mathbf{L}^\infty$ bound of n^h. First, we consider $j=0$ and assume $S(t) = \max\limits_{1\leq i\leq L-1} |n_{i+\frac{1}{2},\frac{1}{2}}(t)|e^{-\tilde{g}'t}$ for $t\in[0,T]$. For the maximum value of S at some index i, we find

$$h^2 \frac{\mathrm{d}|n_{i+\frac{1}{2},\frac{1}{2}}(t)|}{\mathrm{d}t} + h(g_{i+1,\frac{1}{2}}(t)|n_{i+\frac{1}{2},\frac{1}{2}}(t)| - g_{i,\frac{1}{2}}(t)|n_{i-\frac{1}{2},\frac{1}{2}}(t)|) + h(g_{i+\frac{1}{2},1}(t)|n_{i+\frac{1}{2},\frac{1}{2}}(t)| - g_{i+\frac{1}{2},0}(t)|n_{i+\frac{1}{2},-\frac{1}{2}}(t)|) \leq 0,$$

$$h^2 \frac{\mathrm{d}|n_{i+\frac{1}{2},\frac{1}{2}}(t)|}{\mathrm{d}t} + h g_{i+1,\frac{1}{2}}(t)|n_{i+\frac{1}{2},\frac{1}{2}}(t)| - g_{i+\frac{1}{2},0}(t)|n_{i+\frac{1}{2},-\frac{1}{2}}(t)| \leq 0, \quad i=1.$$

and

$$\frac{\mathrm{d}(|n_{i+\frac{1}{2},\frac{1}{2}}(t)|e^{-\tilde{g}'t})}{\mathrm{d}t} + h^{-1} g_{i+\frac{1}{2},1}(t)|n_{i+\frac{1}{2},\frac{1}{2}}(t)|e^{-\tilde{g}'t} \leq h^{-1} g_{i+\frac{1}{2},0}(t)|n_{i+\frac{1}{2},-\frac{1}{2}}(t)|e^{-\tilde{g}'t},$$

By the assumption that $g(x,y,t) \geq g_{\min}(t) \geq g_{\min} > 0$ and $g < K(T+1+\Omega(T))$, we have

$$\frac{\mathrm{d}(|n_{i+\frac{1}{2},\frac{1}{2}}(t)|e^{-\tilde{g}'t})}{\mathrm{d}t} + h^{-1} g_{\min}(t)|n_{i+\frac{1}{2},\frac{1}{2}}(t)|e^{-\tilde{g}'t} \leq h^{-1} \left(\frac{g_{\min}(t)}{g_{\min}}\right) \max_{1\leq i\leq L-1} |g_{i+\frac{1}{2},0}(t) n_{i+\frac{1}{2},-\frac{1}{2}}(t)|. \tag{A.18}$$

Finally, defining $G(t) = h^{-1}\int_0^t g_{\min}(s)\mathrm{d}s$ yields

$$\frac{\mathrm{d}(|n_{i+\frac{1}{2},\frac{1}{2}}(t)|e^{-\tilde{g}'t}e^{G(t)})}{\mathrm{d}t} \leq \frac{1}{h} \left(\frac{g_{\min}(t)}{g_{\min}}\right) \max_{1\leq i\leq L-1} |g_{i+\frac{1}{2},0}(t) n_{i+\frac{1}{2},-\frac{1}{2}}(t)|e^{G(t)}.$$

From the $\mathbf{L}^1$ bound, we can deduce

$$\max_t \max_{1\leq i\leq L-1} |g_{i+\frac{1}{2}}(t) n_{i+\frac{1}{2},-\frac{1}{2}}(t)| \leq h^2 \tilde{B} e^{MT} \|n^h(0)\|_1 \leq \tilde{B} e^{MT} \|n(0)\|_1, \quad t>0$$

and conclude that for the function $S(t)e^{G(t)}$

$$S(t)e^{G(t)} \leq S(0) + \frac{1}{g_{\min}} \tilde{B} e^{MT} \|n(0)\|_1 (e^{G(t)} - 1), \tag{A.19}$$

and $S(t) \leq \max\limits_{1\leq i\leq L-1} \{n_{i+\frac{1}{2},\frac{1}{2}}(0), \frac{1}{g_{\min}} \tilde{B} e^{MT} \|n(0)\|_1\}$, which then gives the $\mathbf{L}^\infty$ bound for the pointwise solution n^h when $j=0$.

Now, we estimate $|n_{i+\frac{1}{2},j+\frac{1}{2}}(t)|$ by first defining $P(t) \equiv \max_{0\le i\le L-1,0\le j\le i-1}\{|n_{i+\frac{1}{2},j+\frac{1}{2}}(t)|e^{-2\tilde{g}'t}\}$. At a fixed time t, specific values of i and j define $P(t)$. If the maximum occurs at $j=0$, $P(t)=S(t)e^{-\tilde{g}'t}$. If the maximum occurs at $i-1>j>0$, we have

$$\begin{aligned} h\frac{\mathrm{d}}{\mathrm{d}t}(|n_{i+\frac{1}{2},j+\frac{1}{2}}(t)|e^{-2\tilde{g}'t}) = -\Big[&g_{i,j+\frac{1}{2}}(t)|n_{i+\frac{1}{2},j+\frac{1}{2}}(t)| - g_{i+1,j+\frac{1}{2}}(t)|n_{i+\frac{1}{2},j+\frac{1}{2}}(t)| \\ &+g_{i+\frac{1}{2},j}(t)|n_{i+\frac{1}{2},j+\frac{1}{2}}(t)| - g_{i+\frac{1}{2},j+1}(t)|n_{i+\frac{1}{2},j+\frac{1}{2}}(t)| + 2h\tilde{g}'|n_{i+\frac{1}{2},j+\frac{1}{2}}(t)|\Big] e^{-2\tilde{g}'t} \le 0, \end{aligned} \tag{A.20}$$

while if the maximum occurs at $j=i-1>0$, we have

$$\frac{\mathrm{d}}{\mathrm{d}t}(|n_{i+\frac{1}{2},j+\frac{1}{2}}(t)|e^{-2\tilde{g}'t}) \le \left[h^{-1}\left(g_{i+\frac{1}{2},j}(t) - g_{i+1,j+\frac{1}{2}}(t)\right)|n_{i+\frac{1}{2},\frac{1}{2}}(t)| - 2\tilde{g}'|n_{i+\frac{1}{2},j+\frac{1}{2}}(t)|\right] e^{-2\tilde{g}'t} \le 0. \tag{A.21}$$

In Eqs. A.20 and A.21, i,j are the maximizing indices that define $P(t)$.

For any $t\in(0,T]$ we can find a minimum $\tilde{t}<t$ such that $P(v)>S(v)e^{-\tilde{g}'v}$ for $v\in(\tilde{t},t]$. If $\tilde{t}=0$, and since $P(t)$ is nonincreasing from Eq. A.21, $P(t)\le P(0)=\|n^h(0)\|_\infty$. If $t>\tilde{t}>0$, $P(t)\le P(\tilde{t})\le S(\tilde{t})\le \max_{0\le t\le T} S(t)$, while if $\tilde{t}=t$, $P(t)=S(t)\le \max_{0\le t\le T} S(t)$. Thus, $P(t)=\|n^h(t)\|_\infty e^{-2\tilde{g}'t}\le \max\{\max_{0\le t\le T}\{S(t)\},\|n^h(0)\|_\infty\}$ and

$$\|n^h(t)\|_\infty \le \max\{\max_{0\le t\le T}\{S(t)\},\|n^h(0)\|_\infty\}e^{2\tilde{g}'t}, \tag{A.22}$$

giving the second conclusion in Theorem A.2 that the $\mathbf{L}^\infty$ bound is uniform and independent of h.

A.2.2. Existence of the weak solution. For a given time $T<\infty$, we can take the grid size $h(k)=\Omega(T)/k\to 0$ by letting the integer $k\to\infty$. Spatially piecewise constant functions can then be defined based on the sequence of vector functions $\{n^{h(k)}\}$. By setting $n^h_{i+\frac{1}{2},i+\frac{1}{2}}(t)=0$, we define $n^h(x,y,t)$, β^h, and $\tilde{\beta}^h$ as

$$\begin{aligned} n^h(x,y,t) =& \sum_{i=0}^{k-1}\sum_{j=0}^{i-1} n^h_{i+\frac{1}{2},j+\frac{1}{2}}(t)\mathbb{1}(ih\le x<(i+1)h, jh\le y<(j+1)h), \\ \beta^h(x,y,t) =& \sum_{i=0}^{k-1}\sum_{j=0}^{i} \beta_{i+\frac{1}{2},j+\frac{1}{2}}(t)\mathbb{1}(ih\le x<(i+1)h, jh\le y<(j+1)h), \\ \tilde{\beta}^h(x,y,z,t) =& \sum_{i=0}^{k-1}\sum_{j=0}^{i-1}\sum_{\ell=0}^{i-1} \tilde{\beta}_{i+\frac{1}{2},j+\frac{1}{2}}((\ell+\frac{1}{2})h,t)\mathbb{1}(ih\le x<(i+1)h, jh\le y<(j+1)h, \ell h\le z<(\ell+1)h), \\ n^h(x,0,t) =& n^h_{i+\frac{1}{2},-\frac{1}{2}}(t), \quad ih\le x<(i+1)h, \end{aligned}$$

where above, $h=h(k)$ and $\mathbb{1}$ is the indicator function. Since there is an upper bound for both β and $\tilde{\beta}$, and both $\beta,\tilde{\beta}$ are continuous, we have the following result

$$\begin{aligned} \lim_{k\to\infty}\beta^{h(k)}(x,y,t) \to& \beta(x,y,t)\ a.e. \quad 0\le\beta^{h(k)}\le\|\beta\|_\infty<\infty, \\ \lim_{k\to\infty}\tilde{\beta}^{h(k)}(x,y,z,t) \to& \beta(x,y,z,t)\ a.e. \quad 0\le\tilde{\beta}^{h(k)}\le\|\tilde{\beta}\|_\infty<\infty, \\ \lim_{k\to\infty} n^{h(k)}(x,y,0) \to& n(x,y,0)\ a.e.. \end{aligned}$$

Then, we can apply Theorem A.2 to the piecewise constant solutions $n^{h(k)}$ of Eqs. A.14.

Corollary A.3 Under the conditions of Theorem A.2, for any $t\in[0,T]$ and any h,

$$\int_0^{\Omega(T)}\mathrm{d}y\int_0^{\Omega(T)}\mathrm{d}x\,|n^h(x,y,t)| \le e^{Mt}\int_0^{\Omega(0)}\mathrm{d}y\int_0^{\Omega(0)}\mathrm{d}x\,|n^h(x,y,0)| \tag{A.23}$$

and

$$\|n^h(t)\|_\infty \le \max\{|n(0)|_\infty, Be^{MT}|n(0)|_1\}e^{2\tilde{g}'t}, \tag{A.24}$$

where $B, M, \tilde{g}'$ are defined in Theorem A.2. The proof is the direct consequence of Theorem A.2.

The sequence of piecewise constant functions $\{n^{h(k)}\}$ is uniformly bounded and $n^{h(k)} \in \mathbf{L}^1 \cap \mathbf{L}^\infty([0,\Omega(T)]^2 \cap \{y<x\}\times[0,T))$, so $n^{h(k)}$ are all $\mathbf{L}^2$ functions. There exists a function $n \in \mathbf{L}^2([0,\Omega(T)]^2 \cap \{y<x\}\times[0,T))$ and a subsequence $k_i \to \infty$ that satisfies $n^{h(k_i)} \rightharpoonup n$. Since $\mathbf{L}^2([0,\Omega(T)]^2 \cap \{y<x\}\times[0,T))$ implies $\mathbf{L}^1$ integrability, we can deduce that n is an $\mathbf{L}^1$ function as desired.

To prove $n^{h(k_i)} \rightharpoonup n$, we need only to verify that there exists a subsequence $n^{h(k_i)}$ such that for all test functions $f \in \mathbf{L}^2$, $\int_0^T \mathrm{d}t \int_0^{\Omega(T)} \mathrm{d}x \int_0^x \mathrm{d}y\, n^{h(k_i)} f \to \int_0^T \mathrm{d}t \int_0^{\Omega(T)} \mathrm{d}x \int_0^x \mathrm{d}y\, nf$. Since $\mathbf{L}^2$ space is separable, we have a countable set of basis function $\{b_i(x,y,t)\}$ for the space $\mathbf{L}^2([0,\Omega(T)]^2 \cap \{y<x\}\times[0,T))$. Thus, every $n^{h(k)}$ can be decomposed as $n^{h(k)} = \sum_{i=1}^\infty \alpha_i^k b_i$. The sequence $\{n^{h(k)}\}$ is uniformly $\mathbf{L}^\infty$ bounded, so $\sum \alpha_k^2$ are all uniformly bounded. We can then select a subsequence $\{n^{h(k_i)}\}$ from $\{n^{h(k)}\}$ satisfying $\lim_{i\to\infty} \alpha_j^{k_i} = \alpha_j$ so that $\sum_{i=1}^\infty \alpha_j^2 < \infty$. If we set $n = \sum_{i=1}^\infty \alpha_i b_i$, then, by decomposing any test function $\Psi \in \mathbf{L}^2([0,\Omega(T)]^2 \cap \{y < x\}\times[0,T))$ by $\Psi = \sum_{i=1}^\infty \gamma_i b_i$, we have

$$\lim_{i\to\infty} \left| \int_0^T \mathrm{d}t \int_0^{\Omega(T)} \mathrm{d}x \int_0^x \mathrm{d}y \left(n^{h(k_i)} - n\right) \Psi \right| = \left| \sum_{s=1}^\infty (\alpha_s^{k_i} - \alpha_s)\gamma_s \right| = 0, \tag{A.25}$$

which gives the result $n^{h(k_i)} \rightharpoonup n$.

We can show that n is a weak solution by multiplying the first two of Eqs. A.14 by a test function $\Psi \in \mathbf{C}^1([0,\Omega(T)]^2 \times [0,T))$, $\Psi(x,y,T) = 0, \Psi(x,y,t) = 0, y \ge x$ for which

$$\Psi_{i+\frac{1}{2},j+\frac{1}{2}}(t) \equiv \frac{1}{h^2} \int_{x_i}^{x_{i+1}} \mathrm{d}x \int_{y_j}^{y_{j+1}} \mathrm{d}y\, \Psi(x,y,t), \quad j \le i.$$

For a given $L \in \mathbf{N}^+$ and $h = \frac{\Omega(T)}{L}$,

$$\begin{aligned}
\int_0^T \mathrm{d}t \sum_{i=1}^{L-1}\sum_{j=0}^{i-1} \Big(& h^2 \frac{\mathrm{d}n^h_{i+\frac{1}{2},j+\frac{1}{2}}(t)}{\mathrm{d}t} \Psi_{i+\frac{1}{2},j+\frac{1}{2}}(t) + h\left[g_{i+1,j+\frac{1}{2}}(t) n^h_{i+\frac{1}{2},j+\frac{1}{2}}(t) - g_{i,j+\frac{1}{2}}(t) n^h_{i-\frac{1}{2},j+\frac{1}{2}}\right] \Psi_{i+\frac{1}{2},j+\frac{1}{2}}(t) \\
& + h[g_{i+\frac{1}{2},j+1}(t) n^h_{i+\frac{1}{2},j+\frac{1}{2}}(t) - g_{i+\frac{1}{2},j}(t) n^h_{i+\frac{1}{2},j-\frac{1}{2}}]\Psi_{i+\frac{1}{2},j+\frac{1}{2}}(t) + h^2 \beta_{i+\frac{1}{2},j+\frac{1}{2}}(t) n^h_{i+\frac{1}{2},j+\frac{1}{2}} \Psi_{i+\frac{1}{2},j+\frac{1}{2}}(t) \Big) \\
& = \int_0^T \mathrm{d}t \sum_{i=1}^{L-1} h g_{i+\frac{1}{2},i}(t) n^h_{i+\frac{1}{2},i-\frac{1}{2}}(t) \Psi_{i+\frac{1}{2},i-\frac{1}{2}}(t), \;\; n^h_{i+\frac{1}{2},i+\frac{1}{2}} = 0.
\end{aligned}$$

Integrating the above equation by parts with respect to time, we find

$$\begin{aligned}
& \int_0^T \mathrm{d}t \left[\sum_{i=1}^{L-1}\sum_{j=0}^{i-1} h^2 n^h_{i+\frac{1}{2},j+\frac{1}{2}}(t) \frac{\mathrm{d}\Psi_{i+\frac{1}{2},j+\frac{1}{2}}(t)}{\mathrm{d}t} + h \sum_{i=1}^{L-2}\sum_{j=0}^{i-1} g_{i+1,j+\frac{1}{2}}(t) n^h_{i+\frac{1}{2},j+\frac{1}{2}}(t)(\Psi_{i+\frac{3}{2},j+\frac{1}{2}}(t) - \Psi_{i+\frac{1}{2},j+\frac{1}{2}}(t)) \right. \\
& \qquad \left. + h \sum_{i=1}^{L-1}\sum_{j=0}^{i-2} g_{i+\frac{1}{2},j+1}(t) n^h_{i+\frac{1}{2},j+\frac{1}{2}}(t)(\Psi_{i+\frac{1}{2},j+\frac{3}{2}}(t) - \Psi_{i+\frac{1}{2},j+\frac{1}{2}}(t)) \right] = \\
& -h^2 \sum_{i=0}^{L-1}\sum_{j=0}^{i-1} n^h_{i+\frac{1}{2},j+\frac{1}{2}}(0)\Psi_{i+\frac{1}{2},j+\frac{1}{2}}(0) - h\int_0^T \mathrm{d}t \sum_{i=1}^{L-1} g_{i+\frac{1}{2},0}(t) n^h_{i+\frac{1}{2},-\frac{1}{2}}(t)\Psi_{i+\frac{1}{2},\frac{1}{2}}(t) \\
& \qquad - \int_0^T \mathrm{d}t \sum_{i=1}^{L-1} h g_{i+\frac{1}{2},i}(t) n^h_{i+\frac{1}{2},i-\frac{1}{2}}(t)\Psi_{i+\frac{1}{2},i-\frac{1}{2}}(t) \\
& + h\int_0^T \mathrm{d}t \left[\sum_{i=1}^{L-2} g_{i+1,i+1}(t) n^h_{i+1,i+1}(t)\Psi_{i+1,i+1}(t) + \sum_{i=1}^{L-1}\sum_{j=1}^{i-1} h^2 \beta_{i+\frac{1}{2},j+\frac{1}{2}}(t) n^h_{i+\frac{1}{2},j+\frac{1}{2}}(t)\Psi_{i+\frac{1}{2},j+\frac{1}{2}}(t) \right].
\end{aligned} \tag{A.26}$$

Since $\Psi_{i+\frac{3}{2},j+\frac{1}{2}}(t) - \Psi_{i+\frac{1}{2},j+\frac{1}{2}}(t) = \int_{ih}^{(i+1)h}\mathrm{d}x \int_{jh}^{(j+1)h}\mathrm{d}y \int_x^{x+h}\mathrm{d}s \frac{\partial\Psi}{\partial s}(s,y,t)$, $|n^h|$ is uniformly bounded while g is $\mathbf{C}^1$ continuous. From above we can pick a subsequence in $\{n^{h(k)}\}$, denoted by $n^{h(k_i)} \rightharpoonup n$. We use $n^h = n^{h(k_i)}$ in the above formula. Since $\Psi \in \mathbf{C}^1[0,T]\times[0,\Omega(T)]^2$, given any Ψ we have a positive upper bound $R(\Psi) < \infty$ for Ψ and any of its first derivatives. Thus,

$$\left| \int_0^T \mathrm{d}t \sum_{i=1}^{L-1}\sum_{j=0}^{i-1} \left(h^2 n^{h(k_i)}_{i+\frac{1}{2},j+\frac{1}{2}}(t) \frac{\mathrm{d}\Psi_{i+\frac{1}{2},j+\frac{1}{2}}(t)}{\mathrm{d}t} \right) - \int_0^T \mathrm{d}t \int_0^{\Omega(T)} \mathrm{d}x \int_0^x \mathrm{d}y\, n^{h(k_i)}(x,y,t) \frac{\partial\Psi(x,y,t)}{\partial t} \right| \leq$$
$$\int_0^T \mathrm{d}t \sum_{i=0}^{L-1} \int_{ih}^{(i+1)h} \mathrm{d}x \int_{ih}^x \mathrm{d}y \left| n^{h(k_i)}(x,y,t) \frac{\partial\Psi(x,y,t)}{\partial t} \right|.$$

As $h \to 0$, $|\int_0^T \mathrm{d}t \sum_{i=0}^{L-1} \int_{ih}^{(i+1)h}\mathrm{d}x \int_{ih}^x \mathrm{d}y\, n^{h(k_i)}(x,y,t)\frac{\partial\Psi(x,y,t)}{\partial t}| \to 0$ since $\frac{\partial\Psi}{\partial t}$ and $n^{h(k_i)}$ are all bounded. Moreover,

$$\int_0^T \mathrm{d}t \int_0^{\Omega(T)} \mathrm{d}x \int_0^x \mathrm{d}y\, h^2 n^{h(k_i)}(x,y,t) \frac{\partial\Psi(x,y,t)}{\partial t} \to \int_0^T \mathrm{d}t \int_0^{\Omega(T)} \mathrm{d}x \int_0^x \mathrm{d}y\, h^2 n(x,y,t) \frac{\partial\Psi(x,y,t)}{\partial t} \tag{A.27}$$

so that the first term in Eq. A.26 tends to the limit in Eq. A.27. By the same procedure and using the condition that g is uniformly continuous in $[0,T]\times[0,\Omega(t)]^2$ (g is $\mathbf{C}^1$), it is easy to verify that the second and third terms on the LHS of Eq. A.26 tend to $\int_0^T \mathrm{d}t \int_0^{\Omega(T)} \mathrm{d}x \int_0^x \mathrm{d}y\, (gn)(x,y,t)\frac{\partial\Psi}{\partial x}$ and $\int_0^T \mathrm{d}t \int_0^{\Omega(T)} \mathrm{d}x \int_0^x \mathrm{d}y\, (gn)(x,y,t)\frac{\partial\Psi}{\partial y}$, respectively.

It is also easy to verify that the first and second terms on the RHS of A.26 tend to $-\int_0^T \mathrm{d}t \int_0^{\Omega(T)} \mathrm{d}x \int_0^x \mathrm{d}y\, n(x,y,0)\Psi(x,y,0)$ and $-2\int_0^T \mathrm{d}t \int_0^\infty \mathrm{d}x \int_0^x \mathrm{d}y \int_0^x \mathrm{d}z\, \Psi(z,0,t)\tilde{\beta}(x,y,z,t)n(x,y,t)$, respectively. The third term on the RHS of A.26 $h\int_0^T \mathrm{d}t \sum_{i=1}^{L-1} g_{i+\frac{1}{2},i}(t) n^h_{i+\frac{1}{2},i-\frac{1}{2}}(t)\Psi_{i+\frac{1}{2},i-\frac{1}{2}}(t)$ tends to 0 since Ψ is $\mathbf{C}^1$ continuous and is 0 on the boundary $x = y$. Since Ψ is continuous and is 0 at $x = \Omega(T)$, $h\int_0^T \sum_{j=0}^{L-2} g_{L,j+\frac{1}{2}}(t) n^h_{L-\frac{1}{2},j+\frac{1}{2}}(t)\Psi_{L-\frac{1}{2},j+\frac{1}{2}}(t)\mathrm{d}t \to 0$ as $h \to 0$. Finally, the last term on the RHS of of A.26 $h\int_0^T \sum_{i=1}^{L-1}\sum_{j=0}^{i-1} h^2\beta_{i+\frac{1}{2},j+\frac{1}{2}}(t) n^h_{i+\frac{1}{2},j+\frac{1}{2}}(t)\Psi_{i+\frac{1}{2},j+\frac{1}{2}}(t)\mathrm{d}t \to \int_0^T \mathrm{d}t \int_0^{\Omega(T)} \mathrm{d}x \int_0^x \mathrm{d}y\, \beta(x,y,t)n(x,y,t)\Psi(x,y,t)$.

By passing to the limit $h \to 0$, we conclude that n exactly satisfies the condition of a weak solution in A.4. Since the numerical solution obtained by the scheme in Appendix B is a discretization in time for the ODE system A.14 it is an approximation to the solution of A.14. Provided $h, \Delta t \to 0$ satisfies the CFL condition $2\|g\|_\infty \Delta t < h$, conclude that at least a subsequence of the numerical solutions converge to the unique weak solution of A.1. Furthermore, recently, the existence to an eigenpair of the adder-sizer PDE A.1 under specific smooth conditions satisfied by the coefficients $g, \beta, \tilde{\beta}$ has been proved in [10], allowing for studying asymptotic behavior of the solution.

Appendix B. Numerical Scheme. We denote $\mathbf{u}(t) = \{\mathbf{n}_1(t), \mathbf{n}_2(t), \ldots, \mathbf{n}_{L-1}(t)\}^\intercal$ where $\mathbf{n}_j(t) = \{n_{\frac{1}{2},j-\frac{1}{2}}, n_{1+\frac{1}{2},j-\frac{1}{2}}, \ldots, n_{L-\frac{1}{2},j-\frac{1}{2}}\}$ and $n_{i\leq j} = 0$. Equations 2.17 and 2.18 can then be written in the form $\mathbf{u}(t+\Delta t) = \mathbf{A}(t)\mathbf{u}(t)$, where

$$\mathbf{A}(t) = \begin{bmatrix} \mathbf{B}_1+\mathbf{C}_1 & \mathbf{C}_2 & \mathbf{C}_3 & \mathbf{C}_4 & \cdots & \mathbf{C}_{L-2} & \mathbf{C}_{L-1} \\ \mathbf{D}_2 & \mathbf{B}_2 & 0 & 0 & \cdots & 0 & 0 \\ 0 & \mathbf{D}_3 & \mathbf{B}_3 & 0 & \cdots & 0 & 0 \\ \vdots & \vdots & \vdots & \vdots & \vdots & \vdots & \vdots \\ 0 & 0 & 0 & 0 & \cdots & \mathbf{B}_{L-2} & 0 \\ 0 & 0 & 0 & 0 & \cdots & \mathbf{D}_{L-1} & \mathbf{B}_{L-1} \end{bmatrix}, \tag{B.1}$$

is made up of the following $L-1$ $L\times L$ matrices

$$\mathbf{B}_i = \left[\begin{array}{c|c} 0\ (i\times i) & 0\ (i\times(L-i)) \\ \hline 0\ ((L-i)\times i) & \mathbf{b}_i \end{array}\right], \quad \mathbf{C}_i = \left[\begin{array}{c|c} 0\ (1\times i) & 0\ (1\times(L-i)) \\ \hline 0\ ((L-1)\times i) & \mathbf{c}_i \end{array}\right],$$

$$\text{and} \quad \mathbf{D}_i = \left[\begin{array}{c|c} 0\ (i\times i) & 0\ (i\times(L-i)) \\ \hline 0\ ((L-i)\times i) & \mathbf{d}_i \end{array}\right],$$

in which $\mathbf{b}_i$ is a lower bidiagonal matrix with diagonal

$$\text{diag}(\mathbf{b}_i) = 1 - \frac{1}{h}g_{j+1,i-\frac{1}{2}}(t)\mathrm{d}t - \frac{1}{h}g_{j+\frac{1}{2},i}(t)\mathrm{d}t - \beta_{j+\frac{1}{2},i-\frac{1}{2}}(t)\mathrm{d}t, \quad j = i, i+1, \ldots, L-1, \tag{B.2}$$

and lower off diagonal $(\mathbf{b}_i)_{-1} = g_{j,i-\frac{1}{2}}(t)\frac{\mathrm{d}t}{h}, \quad j = i+1, \ldots, L-1,$

$$(\mathbf{c}_i)_{sj} = \begin{cases} \tilde{\beta}_{i-\frac{1}{2}+j,i-\frac{1}{2}}((s+\frac{1}{2})h,t)\mathrm{d}t, & i+j-s-1>0,\ i+j\le L \\ 0 & \text{otherwise.} \end{cases} \tag{B.3}$$

and $\mathbf{d}_i$ is a diagonal matrix $\text{diag}(\mathbf{d}_i) = g_{j+\frac{1}{2},i-1}(t)\frac{\mathrm{d}t}{h}, \quad j = i, i+1, \ldots, L-1.$

Appendix C. Monte-Carlo Simulations. In this section we describe the implementation of our Monte-Carlo simulations of the process underlying the adder-sizer mechanism. Suppose we have a list of cells at time t denoted by $S(t) = \{c_1(x_i, y_i, t, b_1), ..., c_i(x_i, y_i, t, b_i)\}$, where x_i is cell c_i's volume and y_i is its added volume. The cell's division factor b_i is determined at birth, which is drawn from a uniform distribution $\mathbf{U}(0,1)$.

Suppose we have a β of the form 2.10 and $\tilde{\beta}$ of the form 2.12. We set the maximum allowable time step to $\Delta t = 0.01$ and determine the next state of the system at time t' by the following

- Step 1: For each cell i, calculate its age a_i at time t by the exponential growth law $\frac{\mathrm{d}x}{\mathrm{d}t} = \lambda x$. We require that $G_i = \int_0^{a_i}\gamma(a')\mathrm{d}a' < b_i$ at the beginning of each step for every i.
- Step 2: For each cell, calculate $G_i = \int_0^{a_i+\Delta t}\gamma(a')\mathrm{d}a'$. If $G_i \ge b_i$, then we numerical calculate a Δt_i such that $\int_0^{a_i+\Delta t_i}\gamma(a')\mathrm{d}a' \approx b_i$.
- Step 3: Choose the smallest Δt_i among all possible Δt_is as the new time step, set time $t' = t + \Delta t_i$ and let all cells gain an extra volume $\lambda x_i \Delta t_i$. If there is no such Δt_i, which means $G_i < b_i$ for every i, go to step 5.
- Step 4: Remove cell i from $S(t')$, record its volume x at t', and generate the random numbers r from the distribution $h(r)$ and b^m, b^{m+1} from $\mathbf{U}(0,1)$. Then, add two new cells in $S(t')$ labeled by $c_m(rx, 0, t, b^m)$ and $c_{m+1}(x - rx, 0, t, b^{m+1})$.
- Step 5: If $G_i < b_i$ for all i, set $t = t'$ and let all cells gain an extra volume $\lambda x_i \Delta t_i$.
- Step 6: Return to step 1 until $t' > t_{\max}$, the maximum time of the simulation.

Here, we set the initial added volume of all cells to zero so the condition in step 1 above is automatically satisfied at $t = 0$. For our runs, we used 10 cells of initial volume 0.5 and $t_{\max} = T$ is the same as the maximum time for the numerical PDE experiments. We can also generalize the model to incorporate the mother-daughter growth coefficient correlation by including a new label λ_i to each cell.

REFERENCES

[1] E. Bernard, M. Doumic, and P. Gabriel, *Cyclic asymptotic behaviour of a population reproducing by fission into two equal parts*, (2016).

[2] J. Betschinger and J. A. Knoblich, *Dare to be different: asymmetric cell division in drosophila, C. elegans and vertebrates*, Current Biology, 14 (2004), pp. R674–R685.

[3] C. Cadart, S. Monnier, J. Grilli, P. J. Sáez, N. Srivastava, R. Attia, E. Terriac, B. Baum, M. Cosentino-Lagomarsino, and M. Piel, *Size control in mammalian cells involves modulation of both growth rate and cell cycle duration*, Nature Communications, 9 (2018), p. 3275.

[4] D. Chandler-Brown, K. M. Schmoller, Y. Winetraub, and J. M. Skotheim, *The Adder Phenomenon Emerges from Independent Control of Pre- and Post-Start Phases of the Budding Yeast Cell Cycle*, Current Biology, 27 (2017), pp. 2774–2783.

[5] T. Chou and C. D. Greenman, *A Hierarchical Kinetic Theory of Birth, Death and Fission in Age-Structured Interacting Populations*, Journal of Statistical Physics, 164 (2016. PMCID: PMC3894939), pp. 49–76.

[6] M. Delarue, D. Weissman, and O. Hallatschek, *A simple molecular mechanism explains multiple patterns of cell-size regulation*, PLoS ONE, 12 (2017), p. e0182633.

[7] M. Doumic, M. Hoffmann, N. Krell, and L. Robert, *Statistical estimation of a growth-fragmentation model observed on a genealogical tree*, Bernoulli, 21 (2015), pp. 1760–1799.

[8] M. Doumic, B. Perthame, and J. P. Zubelli, *Numerical solution of an inverse problem in size-structured population dynamics*, Inverse Problems, 25 (2009), p. 045008.

[9] H. V. Foerster, *Some remarks on changing populations*, Kinetics of Cellular Proliferation Grune and Stratton, (1959), pp. 382–407.

[10] P. Gabriel and H. Martin, *Steady distribution of the incremental model for bacteria proliferation*, Networks & Heterogeneous Media, 14 (2019), p. 149.

[11] C. D. Greenman, *A path integral approach to age dependent branching processes*, Journal of Statistical Mechanics: Theory and Experiment, 2017 (2017), p. 033101.

[12] C. D. Greenman and T. Chou, *Kinetic theory of age-structured stochastic birth-death processes*, Physical Review E, 93 (2016), p. 012112.

[13] M. Guo, L. Y. Jan, and Y. N. Jan, *Control of Daughter Cell Fates during Asymmetric Division: Interaction of Numb and Notch*, Neuron, 17 (1996), pp. 27–41.

[14] H. R. Horvitz and I. Herskowitz, *Mechanisms of asymmetric cell division: two Bs or not two Bs, that is the question*, Cell, 68 (1992), pp. 237–255.

[15] M. Iannelli, *Mathematical theory of age-structured population dynamics*, Giardini editori e stampatori in Pisa, (1995).

[16] M. D. Jauffret and P. Gabriel, *Eigenelements of a general aggeregation-fragmentation model*, Mathematical Models and Methods in Applied Sciences, 20 (2010), pp. 757–783.

[17] D. A. Kessler and S. Burov, *Effective Potential for Cellular Size Control*, arXiv:1701.01725, (2017).

[18] J. Lin and A. Amir, *The effects of stochasticity at the single-cell level and cell size control on the population growth*, Cell Syst, 5 (2017).

[19] A. G. McKendrick, *Applications of mathematics to medical problems*, Proc. Edinburgh Math. Soc., 44 (1926), pp. 98–130.

[20] J. A. J. Metz and O. Diekmann, *The Dynamics of Physiologically Structured Populations*, Springer, 1986.

[21] S. Modi, C. A. Vargas-Garcia, K. R. Ghusinga, , and A. Singh, *Analysis of Noise Mechanisms in Cell-Size Control*, Biophysical Journal, 112 (2017), pp. 2408–2418.

[22] B. Perthame, *Introduction to structured equations in biology*, 2008.

[23] L. Robert, M. Hoffmann, N. Krell, S. Aymerich, J. Robert, , and M. Doumic, *Division in Escherichia coli is triggered by a size-sensing rather than a timing mechanism*, BMC Biology, 12 (2014), p. 17.

[24] M. Schaechter, O. Maaloe, and N. O. Kjeldgaard, *Dependency on medium and temperature of cell size and chemical composition during balanced grown of Salmonella typhimurium.*, Journal of General Microbiology, 19 (1958), pp. 592–606.

[25] F. Si, G. Le Treut, J. T. Sauls, S. Vadia, P. A. Levin, and S. Jun, *Mechanistic origin of cell-size control and homeostasis in bacteria*, Current Biology, 29 (2019), pp. 1760–1770.

[26] J. W. Sinko and W. Streifer, *A New Model for Age-size Structure of a Population*, Ecology, 48 (1967), pp. 910–918.

[27] L. Sompayrac and O. Maaloe, *Autorepressor model for control of DNA replication*, Nat New Biol, 241 (1973), pp. 133–135.

[28] S. Taheri-Araghi, S. Bradde, J. T. Sauls, N. S. Hill, P. A. Levin, J. Paulsson, M. Vergassola, and S. Jun, *Cell-size control and homeostasis in bacteria*, Current Biology, 25 (2015), pp. 385–391.

[29] W. J. Voorn, L. J. Koppes, and N. B. Frover, *Mathematics of cell division in Escherichia coli cell division: comparison between sloppy-size and incremental-size kinetics*, Current Topics in Mol. Genet., 1 (1993), pp. 187–194.

[30] M. Wallden, D. Fange, E. G. Lundius, Özden Baltekin, and J. Elf, *The synchronization of replication and division cycles in individual E. coli cells*, Cell, 166 (2016), pp. 729–739.